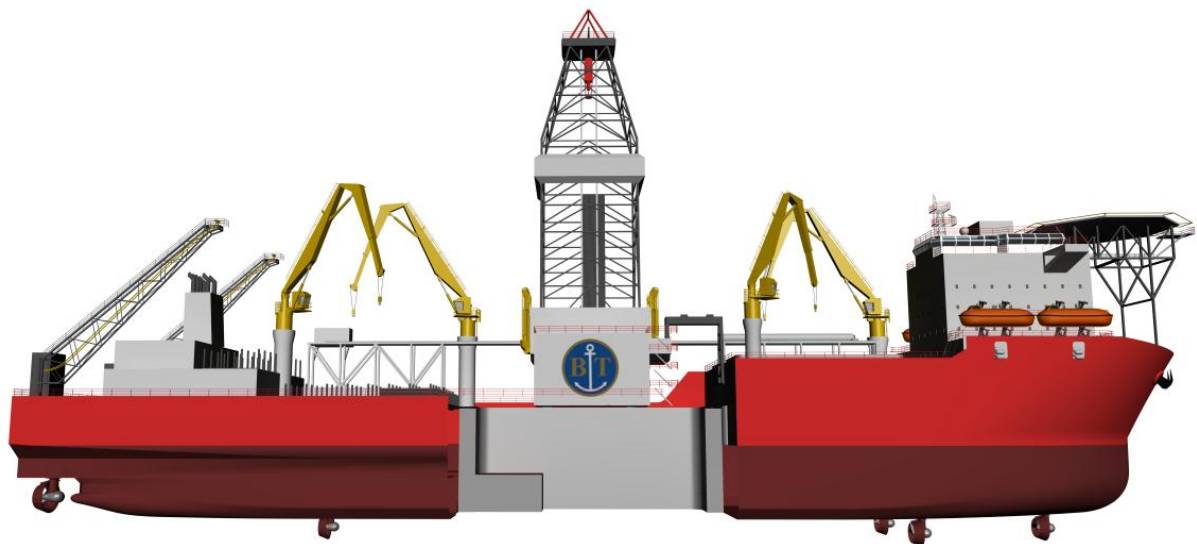


CHALMERS



Effect of the Moonpool on the Total Resistance of a Drillship

Master of Science Thesis

Erik Hammargren

John Törnblom

Department of Shipping and Marine Technology

Division of Marine Design

CHALMERS UNIVERSITY OF TECHNOLOGY

Gothenburg, Sweden, 2012

Report No. X-12/283

A THESIS FOR THE DEGREE OF MASTER OF SCIENCE

Effect of the Moonpool on the Total Resistance of a Drillship

Erik Hammargren

John Törnblom



Department of Shipping and Marine Technology

CHALMERS UNIVERSITY OF TECHNOLOGY

Gothenburg, Sweden 2012

Effect of the Moonpool on the Total Resistance of a Drillship

Erik Hammargren

John Törnblom

© Erik Hammargren & John Törnblom, 2012

Report No. X-12/283

Department of Shipping and Marine Technology

Chalmers University of Technology

SE-412 96 Gothenburg

Sweden

Telephone +46 (0)31-772 1000

Printed by Chalmers Reproservice

Gothenburg, Sweden, 2012

Effect of the Moonpool on the Total Resistance of a Drillship

Erik Hammargren

John Törnblom

Department of Shipping and Marine Technology

Chalmers University of Technology

ABSTRACT

Open moonpools in a drillship is causing additional resistance when the ship is in transit. In previous studies found in literature the resistance increase and the flow behavior has been investigated both with the help of commercial CFD programs but mainly through model tests. It was shown that the water inside the moonpool started to oscillate at forward speed. Two types of oscillation modes, piston and sloshing, has shown to be apparent where sloshing was dominant in longer moonpools and piston in shorter. The amplitude is correlated with the forward speed such that increased forward speed leads to increased amplitudes.

In this thesis the behavior of the flow has been investigated by open source Computational Fluid Dynamic (CFD) software OpenFOAM and a two-dimensional case was set up. For validation, simulations have been carried out on similar models as used in a model test conducted by SAMSUNG Heavy Industries CO LTD (SHI).

The method described in this thesis is a good tool for getting an understanding of the flow behavior and can be used in an early design stage of a moonpool. Results in this report shows that the flow pattern is consistent between model tests and the numerical solution, but it has not been possible to show trends for the resistance in two dimensions.

Key words: OpenFOAM, Moonpool, Drillship, Multiphase flow, Computational Fluid Dynamics (CFD), Ship resistance.

ACKNOWLEDGEMENTS

First we would like to acknowledge *Bassoe Technology* for their support in this thesis, giving us access to computers and also a workplace where all of the analysis and writing has been carried out. A special thanks to M.Sc. David Durling for being the initiator of the subject for the thesis but also, M.Sc. Gustav Andersson for giving useful input and being available for discussion when needed.

Second we would like to thank Prof. Rickard Bensow which supervised the thesis with great interest, for always being available for questions and helping us with the profile of the thesis when needed. We would also like to acknowledge Dr. Abolfazl Shiri, from the Department of shipping and Marine Technology at Chalmers University, for his input on the numerical simulations in OpenFOAM and general CFD acquirements with great interest.

Gothenburg, May 2012

Erik Hammargren

John Törnblom

TABLE OF CONTENTS

ABSTRACT	1
ACKNOWLEDGEMENTS	3
ABBREVIATIONS	7
TABLE OF FIGURES	9
1 INTRODUCTION	11
1.1 BACKGROUND	11
1.2 AIMS AND OBJECTIVES	11
1.3 CLARIFICATION OF THE STUDY	11
1.4 DELIMITATIONS	11
1.5 METHOD.....	11
2 DESCRIPTION OF MOONPOOL CHARACTERISTICS	13
2.1 DECOMPOSITION OF RESISTANCE OF A DRILLSHIP	14
2.2 ORIGIN OF RESISTANCE AND WAVE DEVELOPMENT IN A MOONPOOL	15
3 RECENT WORK	17
3.1 NUMERICAL MODELING	17
3.2 MITIGATION DEVICES	18
4 PATENTS OF MOONPOOL DEVICES	23
5 COMPUTATIONAL FLUID DYNAMICS	27
5.1 GOVERNING EQUATIONS	27
5.2 TURBULENCE MODELING.....	27
5.3 COURANT–FRIEDRICHS–LEWY CONDITION (CFL)	29
5.4 VOLUME OF FLUID METHOD	29
5.5 MODELING AND NUMERICAL ERRORS	30
5.6 MESH.....	31
6 OPENFOAM	33
6.1 BOUNDARY CONDITIONS	35
6.2 UTILITIES AND SOLVERS.....	35
6.3 INTERFOAM	36
6.4 NUMERICAL SCHEMES (FVSCHMES)	36
6.5 SOLUTION ALGORITHM CONTROL (FVSOLUTION)	37
7 CASE SET UP	39
7.1 AIM WITH THE STUDY	39
7.2 PHYSICAL MODELS	39
7.3 GEOMETRY	39
7.4 BOUNDARY CONDITIONS	40
7.5 FLOW CHART	41
7.6 MESH.....	42
8 RESULTS AND DISCUSSION	45
8.1 FLOW FIELD BEHAVIOUR	45
8.2 EVALUATION OF DRAG	51
9 CONCLUSIONS	53
10 FURTHER WORK	55
BIBLIOGRAPHY	57
APPENDIX	59
APPENDIX I – MIN/MAX DRAG AND PRESSURE FOR CASES S0-S3.....	60

ABBREVIATIONS

α	Phase fraction
θ	Inclination angle of flaps
B_m	Breadth of moonpool
C_D	Drag coefficient
CFD	Computational Fluid Dynamics
D	Draught
DoF	Degree of Freedom
DSME	Daewoo Shipbuilding & Marine Engineering Co., Ltd
EHP	Effective Horse Power
F_n	Froude number
NS	Navier Stokes equations
L_C	Half of the cavity depth from the free surface height
L_m	Length of moonpool
L_{pp}	Length of ship
PISO	Pressure Implicit with Splitting of Operators
RANS	Reynolds Averaged Navier Stokes
Re	Reynolds number
R_H	Recess Height
R_L	Recess Length
SHI	Samsung Heavy Industries Co., Ltd.
SIMPLE	Semi-Implicit Method for Pressure-Linked Equations
T_N	Natural period of oscillation
USPTO	United States Patent and Trademark Office
VOF	Volume Of Fluid method

TABLE OF FIGURES

Figure 1. Different types of moonpool configurations	13
Figure 2. Resistance decomposition of a tanker and container ship	14
Figure 3. Flow separation at the moonpool bottom and induced ship motions during transit	15
Figure 4. Excitation of motion due to waves and ship motions in zero velocity condition	15
Figure 5. The optimum moonpool configuration with blocks	17
Figure 6. The domain with explanations	18
Figure 7. Three possible wedge installations on the moonpool.....	19
Figure 8. Flaps in the moonpool opening	20
Figure 9. Graph showing the required shaft power (y-axis) versus ship speed (x-axis) for open moonpool, closed and with flaps.....	20
Figure 10. Damping chambers.....	21
Figure 11. Three different types of moonpool bottoms.....	22
Figure 12. Side view of the moonpool.....	23
Figure 13. Top view of moonpool configurations.....	23
Figure 14. Top view (left) and side view (right) of additional moonpool configurations	24
Figure 15. EHP versus different speed for the different cases	24
Figure 16. Baffle configuration	25
Figure 17. Moonpool plates	25
Figure 18. Speed versus power consumption	26
Figure 19. Patented moonpool plug.....	26
Figure 20. Possible source of errors in computed results using CFD.....	30
Figure 21. A typical case set up in openfoam with case directories.....	34
Figure 22. Geometry with dimensions with variable lengths R_H and R_L for the recess	39
Figure 23. Patches for the square moonpool without modifications.....	40
Figure 24. Mesh for the simulations of the reference case S1.....	42
Figure 25. Comparison of C_D values for different grids	44
Figure 26. Initiation of the vortex at the forward wall	45
Figure 27. Vortex build up	45
Figure 28. Vortex and free surface elevation at its maximum before shedding	46
Figure 29. Initiation of vortex at leading edge, Case S1	47
Figure 30. Vortex Shed and Travels Downstream	47
Figure 31. Travel downstream and redirects flow which enters moonpool	47
Figure 32. Pressure on the aft wall increases as more flow is redirected up in to the moonpool	48
Figure 33. Pressure maxima, Flow is directed upwards by the wall and elevates the free surface	48
Figure 34. Breaking of the freesurface and the initiation of a new vortex at leading edge	48
Figure 35. Completion of the full Sequence	49
Figure 36. Flow pattern for case S4 with no wortex creation at forward wall	49
Figure 37. Flow pattern for case S4 with lowered recess height.....	49
Figure 38. Flow field Simulated in three dimensions from case S1.....	50
Figure 39. Drag force comparison for the different cases S0-S4 (numerical simulation).....	52
Figure 40. The difference in drag force between case S4 and S5 (numerical simulation)	52

1 INTRODUCTION

1.1 BACKGROUND

Bassoe Technology has during the design phase of a drillship studied the effects on the total resistance increase caused by a moonpool. The model tests showed that a moonpool can cause unwanted effects such as considerably increase of the resistance and therefore lower the ship's speed and increase the fuel consumption. Therefore, it is of great interest to get a deep understanding of how the moonpool design affects the resistance of the ship and how it can be improved.

1.2 AIMS AND OBJECTIVES

The aim for this master thesis is to investigate the following subjects:

- Extensive literature study of earlier research covering moonpools, such as model tests, numerical models and patents.
- Finding and running a reference case with Computational Fluid Dynamics (CFD) to validate the software by calculating moonpool resistance and visualization of the flow inside the moonpool.
- Investigate if it is possible to evaluate different moonpool designs with a two-dimensional CFD simulation.
- Study the flow pattern inside the moonpool by studying model tests and numerical methods.

1.3 CLARIFICATION OF THE STUDY

- Extensive literature study:
 - What have been done previously?
 - What approach solving the problem is suitable?
 - What observations have been done on the flow behavior and what is the impact on the resistance?
 - Is it possible to find a reference case to validate results?
 - Are there any patented solutions on moonpool designs?
- How can this flow problem be modeled with CFD?
- Which software is appropriate to use to evaluate this type of fluid dynamic problem?
- Greater understanding of the flow behavior and the origin of the added resistance.

1.4 DELIMITATIONS

The focus of the thesis will be on the design of the moonpool which results in that the hull and propulsion systems will be unchanged. The ship with the moonpool will not be modeled but represented as a two dimensional channel flow with a cavity, since the availability of computational power is limited and it should be sufficient to capture the flow characteristics.

1.5 METHOD

In this thesis CFD-software OpenFOAM is used to model the flow in a moonpool and evaluating different designs with regard to minimizing the resistance. As mentioned before the focus will be on flow behavior in the moonpool. In the CFD simulations, the moonpool is modeled in two dimensions since the available computational power is limited. This gives an understanding of the flow characteristics, even though the side effects from the hull bottom are not included. The thesis also includes an extensive study of previous work on the subject as well as a brief introduction to OpenFOAM and CFD in general.

2 DESCRIPTION OF MOONPOOL CHARACTERISTICS

The moonpool is an opening in the hull which is necessary for drilling pipes and risers to operate. The moonpool can have different shapes varying from a clean rectangular moonpool to more advanced geometries with dampening devices installed. To reduce oscillation and resistance induced during transit, many solutions have been developed; some of them are shown in Figure 1 and will be discussed further in Chapter 3. The most obvious would be to have a hatch which is closed during transit, but this is not preferred by the industry. Since drillships are often chartered at a high daily rate and operates far away from the coastal areas with no docks nearby, a failure to open the hatch would leave the ship inoperable for drilling and lead to a large economic cost.

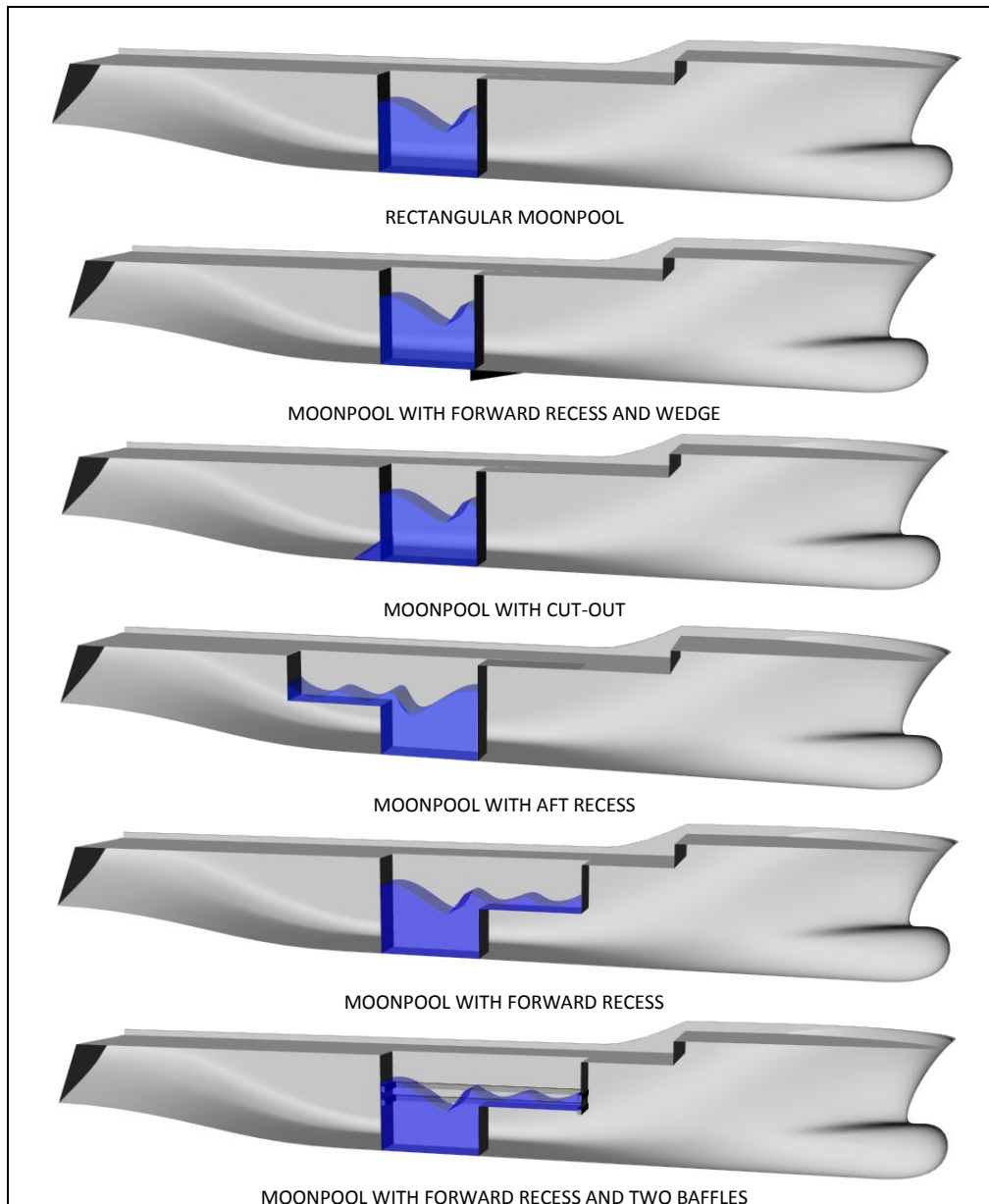


FIGURE 1. DIFFERENT TYPES OF MOONPOOL CONFIGURATIONS

The customization of the moonpool shape is restricted by a number of conditions that comes from both structural as well as operable requirements from the crew and equipment. Under normal circumstances the moonpool will deliver shelter but in some cases, when the oscillations inside the moonpool increase, the waves can be of larger amplitude inside the moonpool than outside.

2.1 DECOMPOSITION OF RESISTANCE OF A DRILLSHIP

The resistance of a drillship in transit mode is to be compared to a tanker and a container ship. Since the drillship is somewhere in between these ships in terms of size and operation velocity an approximation is that it will be somewhere similar to the partition of this type of ships. The tanker operates at the same velocity but at a lower Froude number due to the size differences whereas a container ship, which has the same size, operates at a higher velocity i.e. higher Froude Number (F_n). The F_n is defined as

$$F_n = \frac{V}{\sqrt{gL}} \quad (2.1)$$

where V is the velocity, g is gravitational constant, L is the length of the ship. The overall resistance can be split into wave and viscous resistance. In turn, these two types of resistance can be divided according to Figure 2 for a tanker and container ship respectively.

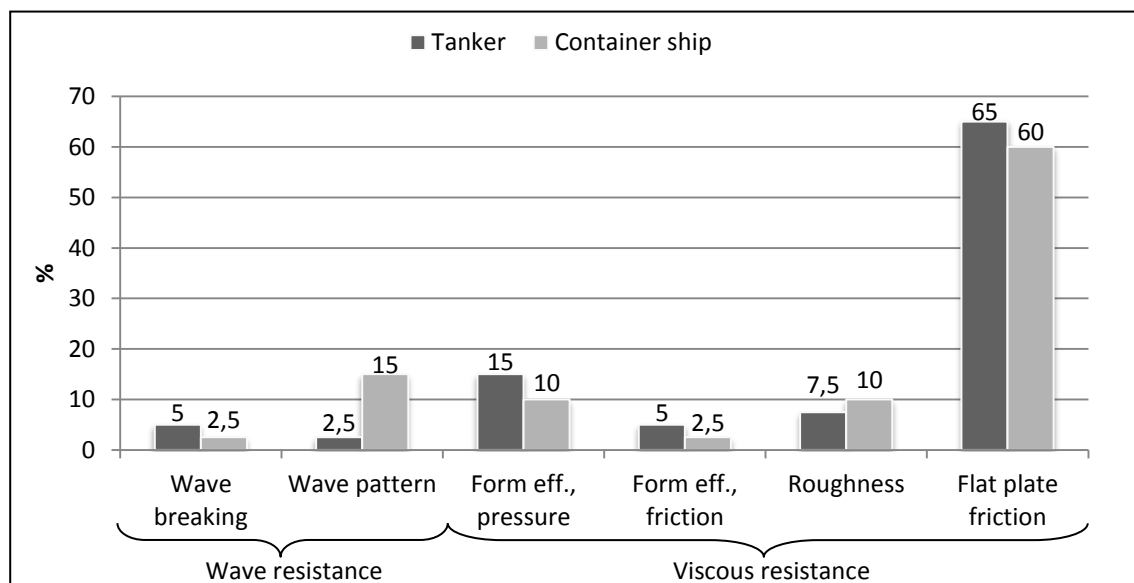


FIGURE 2. RESISTANCE DECOMPOSITION OF A TANKER AND CONTAINER SHIP (FROM LARSSON ET. AL. [1])

It can be observed that the overall resistance is similar between the two types of ships, but since the container ship operates at higher F_n the wave resistance is greater whereas the viscous resistance is greater for the tanker operating at a lower F_n .

In the case of a drillship, the presence of the moonpool will not affect the wave breaking and pattern resistance since the shape of the hull will be unchanged in terms of the interaction with surrounding waves. The form effect from pressure (viscous pressure resistance) originates from boundary layer created along the surface of the ship, which causes displacement of the streamlines along the aft part of the hull. This leads to pressure imbalance and will be further affected by the presence of the moonpool since there will be more disturbances of the flow. When the flow approaches the ship, it has to go around the hull which leads to differences in the local velocity compared to the undisturbed flow ahead of the ship. Since this is not the case of a flat plate, it leads to form effect from friction causing an increase in friction compared to a flat plate. This is a quite small part of the overall resistance but there are more disturbances of the flow with the moonpool present, but at the same time the boundary layer in the aft part gets smaller so the effect on the frictional resistance is not clear. Roughness will be about the same since it has to do with the fouling of the surface which will be unchanged [1].

2.2 ORIGIN OF RESISTANCE AND WAVE DEVELOPMENT IN A MOONPOOL

There are two reasons for water motion in the moonpool, the first is the forward speed of the vessel in transit mode and the second is when waves are approaching the vessel in operating mode, at zero speed [2]. The motion appears as two modes of oscillations, so called piston and sloshing mode. The appearance of the piston mode oscillations is when there is a vertical (heave) motion of the water column, while the sloshing mode is water moving between the vertical walls in longitudinal direction (surge).

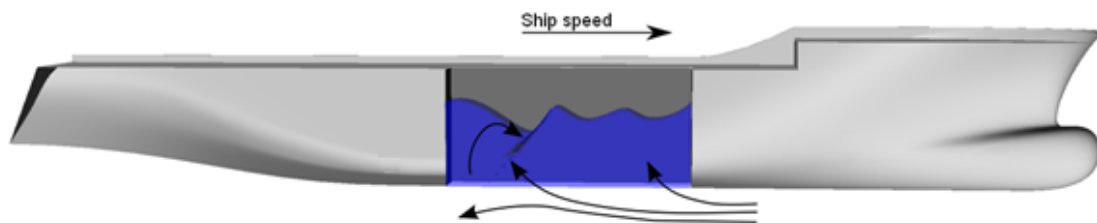


FIGURE 3. FLOW SEPARATION AT THE MOONPOOL BOTTOM AND INDUCED SHIP MOTIONS DURING TRANSIT

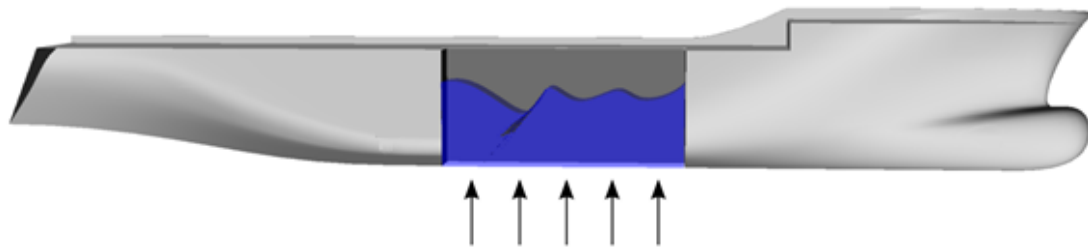


FIGURE 4. EXCITATION OF MOTION DUE TO WAVES AND SHIP MOTIONS IN ZERO VELOCITY CONDITION

When moving at transit speed through calm water the oscillations in the moonpool are initiated by vortices created at the forward edge of the moonpool, by separation of the shear layer. The hairpin like vortices get in contact with the trailing edge of the moonpool and interact with the free surface. As the vortices travel upwards inside the cavity the appearance of sloshing of the free surface is initiated.

For a square moonpool Sadiq & Xiong-liang [3] claims that, at lower F_n numbers, piston mode is initiated when the frequency of the fluid, the natural frequency initiated by the irrotational flow field inside the moonpool and the oscillation frequency of the shear layer is adopting the same value. When the F_n is increased the frequency of shear layer separation and free surface oscillations are not equal and the piston phenomena occurs due to the energy dissipated from the vortices created at the upstream edge of the moonpool. Pressure on the walls of the moonpool is correlated with the ship speed, as the velocity increases the pressure is lowered due to the presence of resonance between free surface oscillation frequency and shear layer oscillation frequency [4].

This leads to viscous effects, such as turbulent vortices dominating the initiation as well as the flow pattern inside of the moonpool. The resonant frequency is mainly dependent on the moonpool geometry while the speed of the ship determines the amplitude of the oscillations. Vortices generated at the forward edge of the moonpool have the same frequency as the oscillation of the water column. When the oscillations of the water column become large they can control the creation of new vortices and lock the system at this frequency, so called phase locking (hysteresis effect). It has also been observed that due to this phase locking phenomena, the violent resonant mode oscillation is sustained over a large speed range [5].

According to model tests performed at Delft University [5] and by SHI [6] it was found that the presence of sloshing will be expected when the ratio between draught and length of the moonpool are

$$\left\{ \begin{array}{ll} \frac{D}{L} < 0.35 \text{ to } 0.39 & (\text{Delft University}) \\ \frac{D}{L} < 0.66 & (\text{SHI}) \end{array} \right.$$

which are in conflict with each other. The reason for this is unknown but could be due to differences in model test setups and varying moonpool configurations. However, the conclusion is that the piston mode oscillation is typically observed in moonpools of shorter length, while sloshing in longer ones.

When trying to optimize the resistance, there are two possible solutions. The first one is trying to avoid vortex creation and the second one reducing water column oscillations by damping. Both solutions aim to minimize the so called sloshing and piston mode oscillation of the free surface. Different possible solutions to optimize the resistance are presented in Chapter 3.

3 RECENT WORK

Historically, most of the research on moonpools has been carried out using experimental methods. Different mitigation devices and geometries have been evaluated to find an optimum solution. More recently, attempts have been made to develop numerical methods for predicting the behavior of the flow in the moonpool by the use of CFD. This chapter will summarize the results from numerical studies and model tests found during the literature study.

3.1 NUMERICAL MODELING

In 2005 Gillarde and Cotteleer [2] made an attempt to model the flow in the moonpool using the software COMFLOW. In their study they managed to get a relatively good reproduction of the flow characteristics, with flow separation on the upstream wall and a clipping vortex entering the back of the moonpool. Based on their results they predicted that future numerical developments using Volume of Fluid (VOF) methods would yield improvements in the numerical predictions of the potential problems.

A further attempt was made in 2007 by SHI [7] who used the software ANSYS FLUENT to predict how the resistance changes for different moonpool shapes with damping blocks. Their approach was to simulate three-dimensional models of five different simplified moonpool geometries. Based on the numerical results, an optimum moonpool was designed and evaluated in calm water model tests. The optimal is the one with three damping blocks shown in Figure 5. Their conclusion is that the numerical method they have developed can be used at an early stage of the moonpool design.

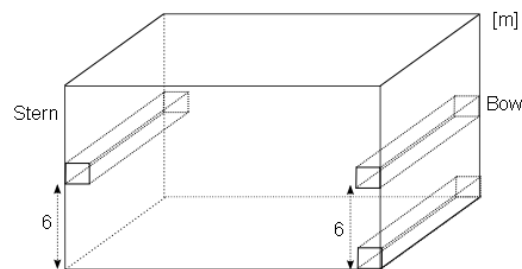


FIGURE 5. THE OPTIMUM MOONPOOL CONFIGURATION WITH BLOCKS (FROM SHI [7])

At the 27th ASME conference on Offshore Mechanics and Arctic Engineering in 2008, two reports regarding the flow in the moonpool were presented. The first report [6] describes how the authors used ANSYS FLUENT to investigate the flow characteristics by using a two-dimensional representation of the moonpool. Their observation is that CFD is a good tool for understanding the flow behavior inside the moonpool, but for evaluating the drag in the three-dimensional case, model tests have to be performed due to the complicated flow phenomena involved. It should be mentioned, based on manufacturing requirements and the results from the two-dimensional CFD analysis, an optimal moonpool design could be decided before conducting the model tests.

The authors of the second report [3] used ANSYS CFX to calculate the flow in both two- and three-dimensions. In the report [3] it is stated that the simulation of a two phase cavity flow is complex because of the massive separation regions and the complex coupling between different flow phenomena leading to large self sustained oscillations. The most important results from the two-dimensional case are that the flow in the moonpool is dependent of the length between the upstream edge of the moonpool and the inflow point. By analyzing the numerical results from the three-dimensional calculations, with the results from experiments it can be seen that the results agree very well until half of the cavity depth from the free surface height, L_c in Figure 6. In the end of the report,

the authors recommend further studies and a development of a 'Best Practice Procedure' to reduce numerical and set up errors when establishing CFD as an industrial tool for this type of flow problems.

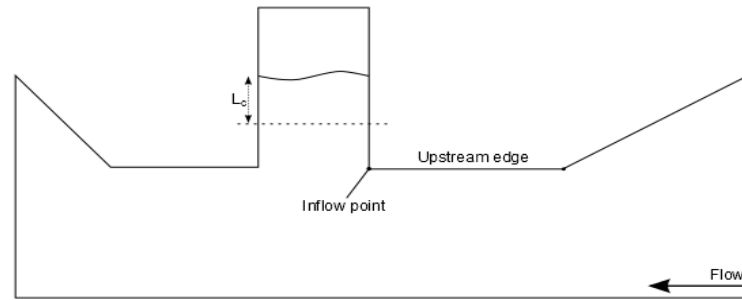


FIGURE 6. THE DOMAIN WITH EXPLANATIONS (FROM SADIQ [3])

The latest report found was written in 2009 by Fukuda and Yoshi [8]. They have used a GSMAC-FEM (Generalized Simplified Marker and Cell – Finite Element Method) for the ALE (Arbitrary Lagrangian – Eulerian) formulation. A method which they describe is accurate for cavity flows with a free surface. It could be observed that the moving amplitude of the free surface is larger for the calculated case, compared with the experimental results. This is believed to be due to the fact that the calculations were made on a two-dimensional model, while the experiments were carried out with three-dimensional ship models. This method was not applicable for geometries where sloshing mode was dominant.

3.2 MITIGATION DEVICES

Most of the mitigation devices described in this chapter is evaluated by model tests. In a few cases numerical methods have been used as aid in an early design stage.

3.2.1 WEDGES AND CUT-OUTS

Wedges under the moonpool will curve the flow downward, carrying vortices away underneath the vessel. This reduces the momentum drag, which is the drag induced by the vortices at the upstream edge. Wedges are effective for shorter moonpools, but fail to reduce resistance for longer designs. The reduction of resistance due to oscillations does not balance the added appendage drag induced from the wedge [5]. In their report from 2008, van't Veer and Tholen [5] discuss when it is beneficial to use a wedge and their main conclusion is that the wedges are best for shorter moonpools with the ratio L_m/D larger than one. They also state that there is limited knowledge on how to design the most efficient wedge. In addition, Gillarde and Cotteleer [2] claim that there is no numerical tool which can aid in the design of the wedge. Instead, the optimum length and angle of the wedge are decided through model tests by trials and errors. For an optimal wedge the angle normally varies between 5° and 15° and the wedge length is to be around 20% of the moonpool length. These dimensions most probably depend on the ship speed together with the length of the moonpool.

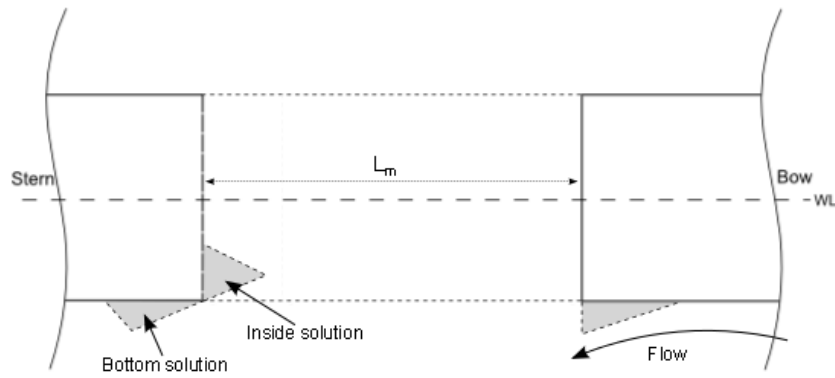


FIGURE 7. THREE POSSIBLE WEDGE INSTALLATIONS ON THE MOONPOOL (FROM ENGLISH [9])

The flow behavior is more complicated for longer moonpools. van 't Veer and Tholen [5] showed, by model tests, that the resistance for longer moonpools can be reduced drastically by implementing a cut-out aft of the moonpool. While model tests on a recess type moonpool performed by SHI, proved that the reduction was very small [6]. This indicates that there is no easy way to answer if a wedge is an efficient solution or not, but one has to consider the overall design of the moonpool.

3.2.2 FLAPS

The idea with flaps is to block the upwelling of vortices into the moonpool and by that reduce the added resistance. It was shown from model tests that having flaps covering the whole opening gave the same result as only covering the aft part in terms of oscillation of waves and added resistance. Since the later gives more clearance in the moonpool, this solution is preferable. An alternative to the grid of flaps is to use a single flap. Gaillard and Cotteleur [2] have carried out model tests with varying length between 30% and 50% of the moonpool length and with different inclinations, ϑ . The longest flap with the lowest inclination showed the best results in terms of reduced resistance and oscillations in the moonpool.

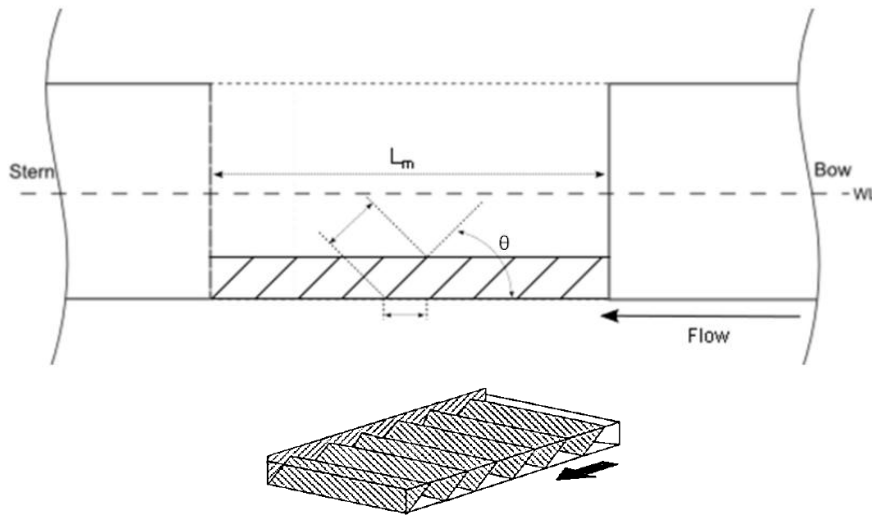


FIGURE 8. FLAPS IN THE MOONPOOL OPENING (FROM GAILLARDE AND COTTELEUR [2])

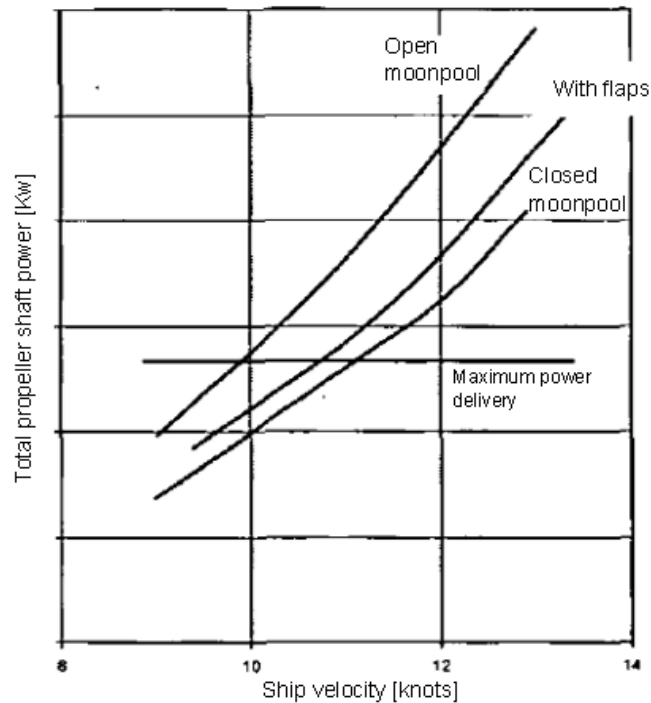


FIGURE 9. GRAPH SHOWING THE REQUIRED SHAFT POWER (Y-AXIS) VERSUS SHIP SPEED (X-AXIS) FOR OPEN MOONPOOL, CLOSED AND WITH FLAPS (FROM GAILLARDE AND COTTELEUR [2])

3.2.3 VERTICAL BULKHEADS

Previous solutions have been based on the principle of obstructing the large vortex originating from flow separation. Another approach is to change the natural frequency of the column of water. This can be done by installing a vertical bulkhead and divide the moonpool into two smaller longitudinal sections. It was shown during model tests that this was a method that gave preferable results [2].

3.2.4 BAFFLES/FLANGES

Three types of flange positions inside the moonpool have been tested, at the free surface, below the free surface and at the opening of the moonpool. The purpose of these installations is to reduce the water oscillations by increasing the damping. It is shown from tests [10] [11] that the moonpool with flanges below the free surface give significant increase in damping in transit compared to the other solutions. SHI has a patented solution for this type of damping device, see Chapter 4.

3.2.5 DAMPING CHAMBERS/DEVICES

This device was tested by Spangenberg and Jacobsen in 1943 [2] and the principle is that when water level rises inside the moonpool, the water motion is damped by longitudinal bulkheads together with damping chambers. When water level decreases the water will travel from the chambers back into the moonpool. This was tested successfully and vertical wave motion is converted into horizontal and wave energy gets dissipated as heat, minimizing the oscillations.

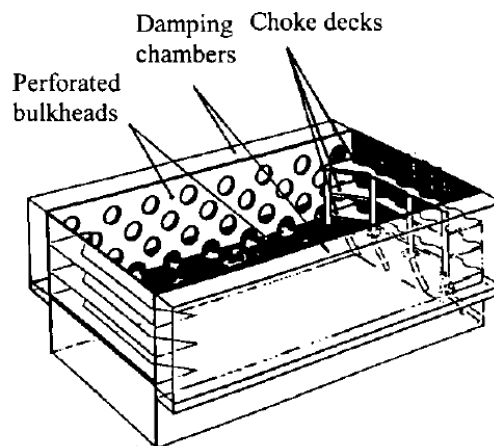


FIGURE 10. DAMPING CHAMBERS (FROM GALLARDE AND COTTELEER [2])

3.2.6 RECESS

The recess, shown in Figure 1, main purpose is for assembling of drilling equipment and transportation of them to the main moonpool. However, it has also advantages in terms of lower resistance, compared to a rectangular non recess moonpool [6]. SHI has applied for a patent on a solution of an aft type recess which is further discussed in Chapter 4. An aft recess has been the main subject of the study in this report and results from SHI's report has been used as reference when validating the results.

3.2.7 MOVING STRUCTURE

As the name implies, this group consists of solutions where a movable structure is used to avoid the flow from entering the moonpool. However, due to high installation costs, maintenance costs and risk of failure this is not a realizable solution for drillships [6].

3.2.8 CONVERGING MOONPOOL BOTTOM

To reduce flow entering the moonpool English [9] suggests the use of a convergent shape of the moonpool opening. This is the total opposite to divergent openings, as often used in aircraft intakes, which is used to increase the amount of flow entering the opening. Model tests have shown a significant reduction of the oscillations and added drag compared to a moonpool with a parallel opening.

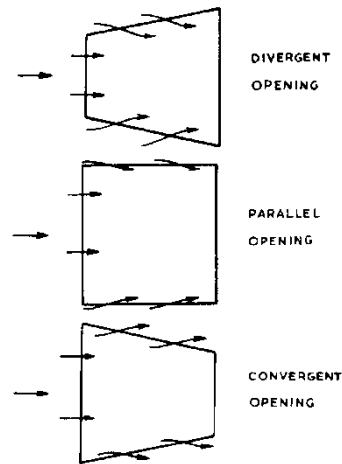


FIGURE 11. THREE DIFFERENT TYPES OF MOONPOOL BOTTOMS (FROM ENGLISH [9])

3.2.9 CHANGING THE DRAUGHT

When changing the draught there is a direct impact on the natural frequency of the water column in transit mode, trying to combine this with the ship speed there is a possibility to reduce the oscillations. The approach would then be to find a draught which interacts with the desired speed in a beneficial way [2].

4 PATENTS OF MOONPOOL DEVICES

During the literature study, a number of different patented solutions have been found for damping devices in moonpools. Some of them are of Class B, which means granted patents and some are patent applications (pending), Class A [12].

SHI has applied for patents for a numerous of different solutions to decrease the fluid movement, by adding an extra space behind the moonpool with varying dimensions. Figure 12 shows the model from side view. The different cases are presented in Figure 13 and shows variation of the aft part of the moonpool. Worth to mention is that these are of Class A1 as of this date (May 10, 2012).

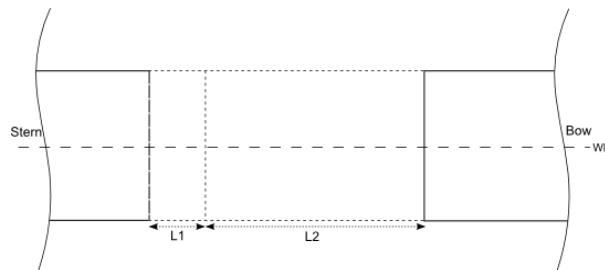


FIGURE 12. SIDE VIEW OF THE MOONPOOL (FROM SHI PATENT [13])

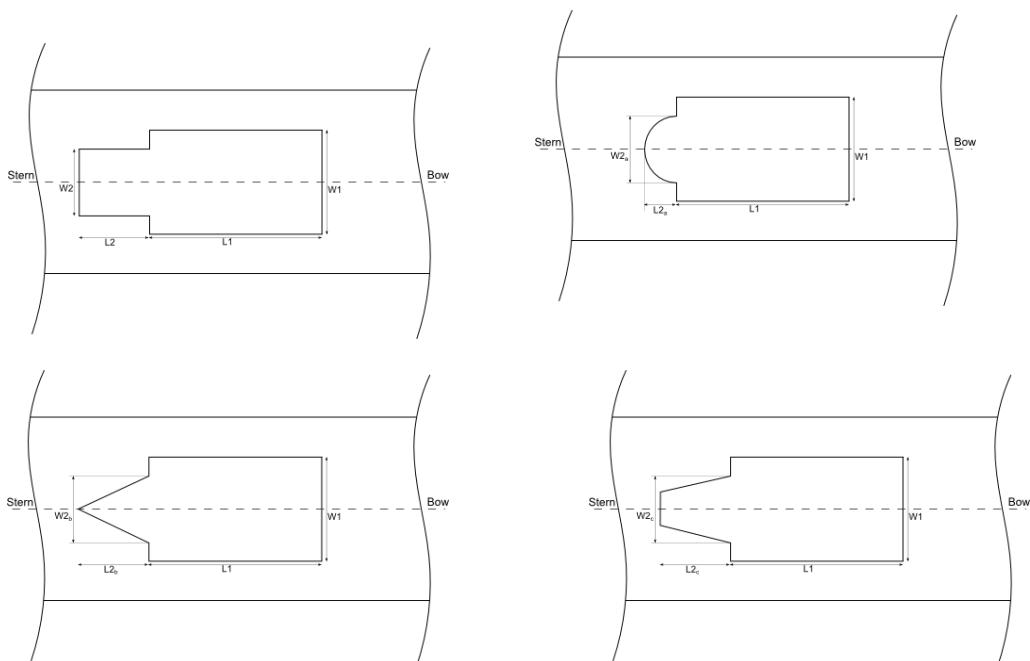


FIGURE 13. TOP VIEW OF MOONPOOL CONFIGURATIONS (FROM SHI PATENT [13])

The patent continues with two other configurations of the moonpool, seen in Figure 14. By installing a partition wall the amplitude of sloshing and free surface movements can be reduced since the length of the moonpool is shortened and thereby the resistance is decreased. By forming an opening towards the backward space of the moonpool with a constant transverse width which is narrower towards the stern of the drillship, there will be a reduction of the amount of seawater flowed into the forward part. This will cause a reduction of the resistance according to the patent. In Figure 15 the results from towing tank experiments is presented and is shown as effective horsepower (EHP) versus ship speed [13].

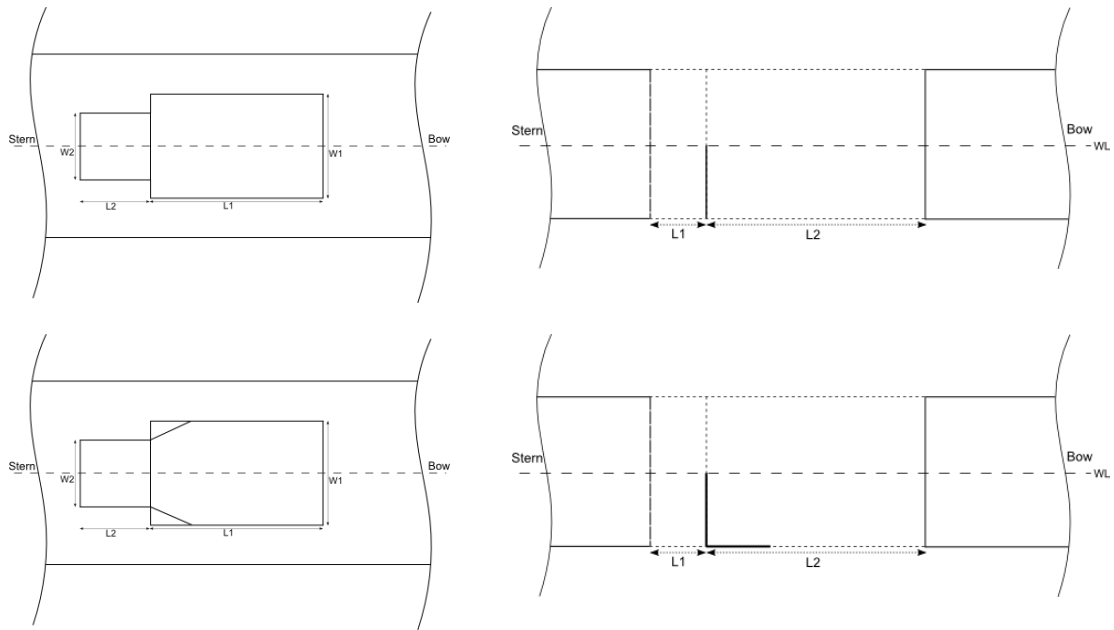


FIGURE 14. TOP VIEW (LEFT) AND SIDE VIEW (RIGHT) OF ADDITIONAL MOONPOOL CONFIGURATIONS (FROM SHI PATENT [13])

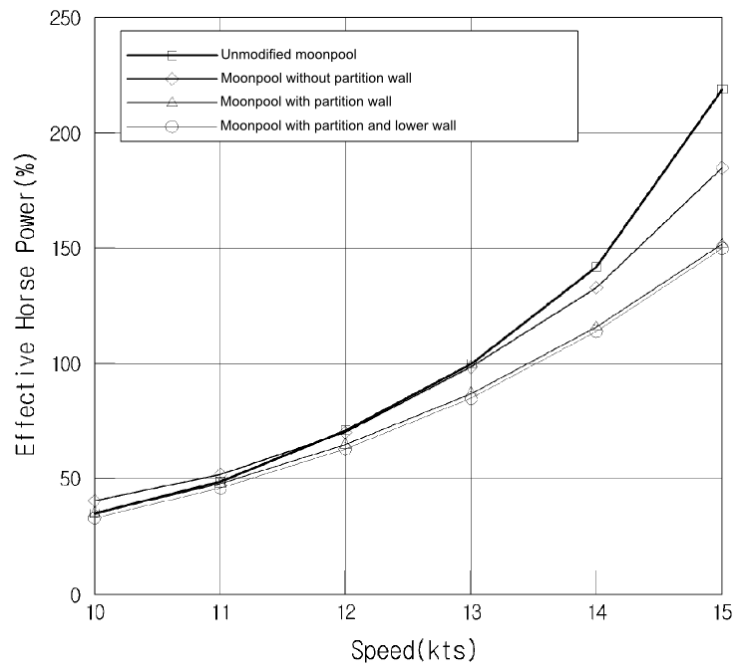


FIGURE 15. EHP VERSUS DIFFERENT SPEED FOR THE DIFFERENT CASES (FROM SHI PATENT [13])

Another patent by SHI, which is granted B2 by USPTO, consists of an anti-sloshing device by introducing baffles on a square moonpool bow and stern walls, opposite sidewalls and a bottom block, see Figure 16. The plates are placed so that, when the ship is in operating mode, are below the free surface and in transit mode the free surface are somewhere in between the plates. The idea behind this solution is to absorb the kinetic energy of water in the moonpool, thus minimize the sloshing, overflow and the vortex creation inside the moonpool [14].

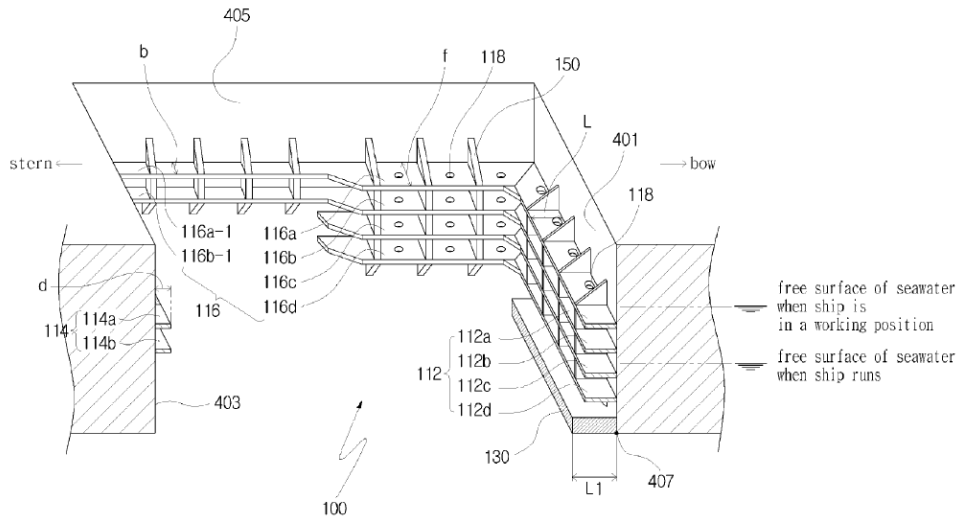


FIGURE 16. BAFFLE CONFIGURATION (FROM SHI PATENT [14])

According to the patent the drawings are only illustrative and do not set the boundaries of the invention by means of dimensions and set ups and also includes the plate holes, used for mitigation of forces in the moonpool, named 118 in Figure 16.

DSME has applied for a patent, currently class A1 (May 14, 2012), for a device that consists of two ramps oriented in the longitudinal direction with horizontal inclined plates, as seen in Figure 17. The plates will be unfolded during operation condition, by hinges which are located at the aft and forward part of the moonpool. The idea behind the plates is to block separated flow going into the moonpool during transit, thus decrease the overall resistance of the ship. The device is described as light weighted and has also the advantage of preventing ice from packing inside the moonpool when operating in polar areas. According to model tests their device will decrease the power consumption drastically compared to a plain moonpool configuration [15].

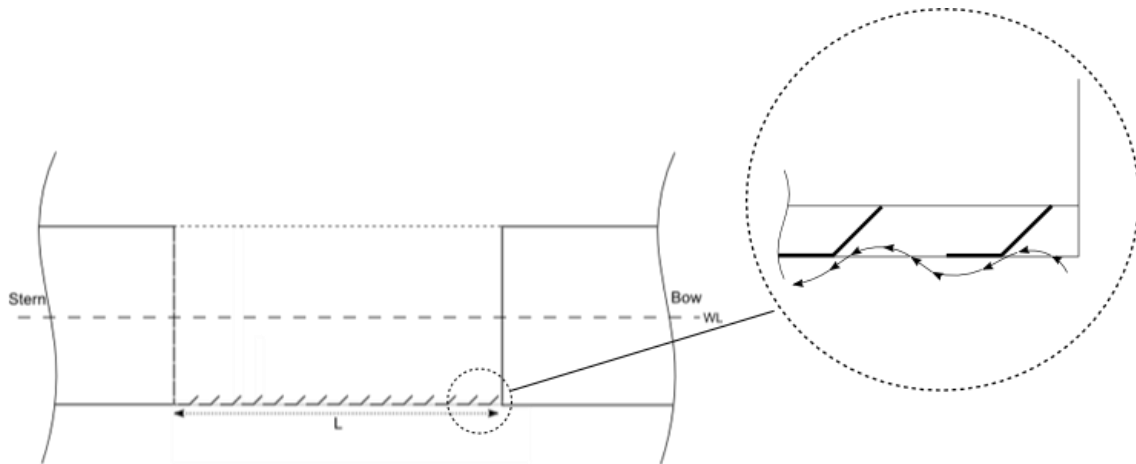


FIGURE 17. MOONPOOL PLATES (FROM DSME PATENT [15])

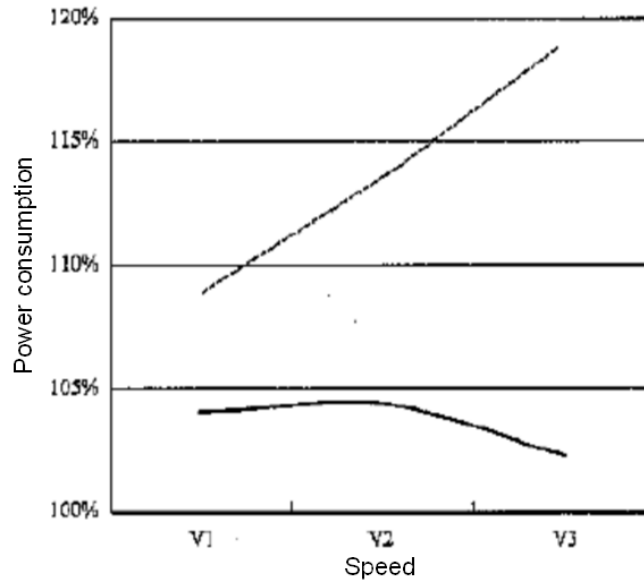


FIGURE 18. SPEED VERSUS POWER CONSUMPTION (FROM DSME PATENT [15])

A patent, classed B2, by Halter Marine, Inc. consists of a buoyant moonpool plug which is used to close the opening during transit. During operational condition the plug is situated on deck and is fit into place by the use of a crane [16].

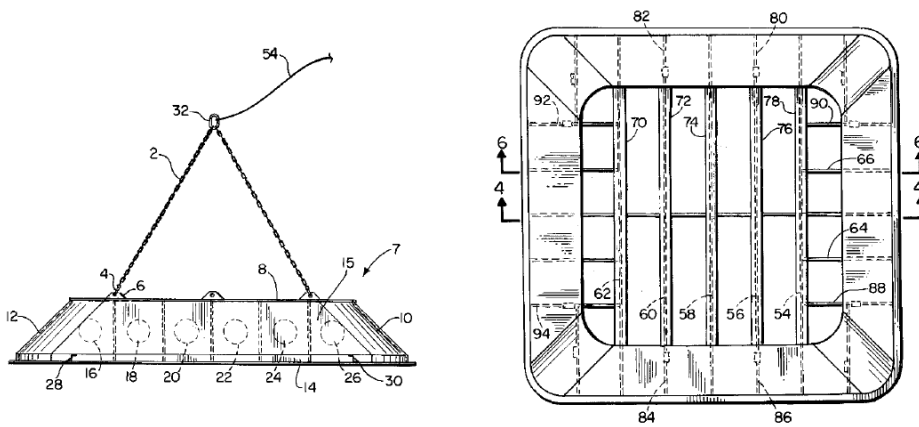


FIGURE 19. PATENTED MOONPOOL PLUG (FROM HALTER MARINE INC PATENT [16])

5 COMPUTATIONAL FLUID DYNAMICS

Computational Fluid Dynamics is a part of fluid dynamics and is used to solve fluid flow problems by the use of numerical methods and algorithms. The reality is represented by a conceptual model which is then discretized to a mathematical model, solved numerically. The governing equation is the Navier-Stokes equation which can be simplified, by neglecting viscosity, to the Euler equations. By removing terms describing vortices the equations can be simplified further, which is the case for the potential solvers. Potential flow is faster and less demanding on computer resources but this has a price neglecting turbulence. The moonpool case has a flow with separation of the shear layer at the leading edge which will affect the appearance of the free surface inside the moonpool; a Reynolds Averaged Navier-Stokes (RANS) method is more suitable where turbulence has a great impact on the flow behavior [1].

5.1 GOVERNING EQUATIONS

The equations which are governing for a multiphase flow are the Reynolds averaged continuity and momentum equations [3];

$$\frac{\partial}{\partial x_i}(\rho_m u_i) = 0 \quad (5.1)$$

$$\frac{\partial}{\partial x_i}(\rho_m u_i u_j) = \frac{\partial}{\partial x_i} \left(\mu_m \left[\frac{\partial u_i}{\partial x_j} + \frac{\partial u_j}{\partial x_i} \right] \right) - \frac{\partial P}{\partial x_j} + \frac{\partial}{\partial x_i} (-\rho_m \overline{u_i' u_j'}) + \rho_m g_j + F_j \quad (5.2)$$

where u_i and u_i' are Reynolds averaged and fluctuating velocity components, respectively, in x_i direction, P is pressure, g is gravity, F_j are body forces due to centrifugal terms and ρ_m, μ_m are the volume-weighted density and viscosity.

To obtain the Reynolds stresses $\rho_m \overline{u_i' u_j'}$ two different closure models are used [3]. The models are described further in Chapter 5.2.

5.2 TURBULENCE MODELING

The Boussinesq assumption is one of the most important in turbulence modeling [1]. The assumption is made that the Reynolds stresses can be computed from the rate of strain tensor in the same way as the viscous stresses are in the Navier-Stokes equations. This is based on the assumption that the turbulent mixing has the same behavior as the viscous mixing and both arises from molecular mixing. A big difference is that the molecular viscosity μ is a known physical constant whereas the turbulent counterpart μ_t is unknown and must be computed at every single point in the computational domain. To calculate μ_t one velocity scale and one length scale must be known. These scales may be obtained in various ways using different turbulence models. To choose which model to use is not an exact science, one must simply try which one fits the problem best. A balance has to be made between accurate enough results and cost in terms of calculation time. However, in Naval Architecture, the two-equation models are the most commonly used and will be discussed further in this report. An overview of other models can be found in the book *Turbulence modeling for CFD* [17].

5.2.1 TWO-EQUATION MODELS

The Two-Equation models are the simplest complete turbulence models. Complete means that they can be used to predict turbulence properties in the flow without any prior knowledge of the turbulence structure [17].

Among the two-equation models there are two of special importance, the $k-\epsilon$ and the $k-\omega$ models. The $k-\epsilon$ model has traditionally been the most popular choice in ship hydrodynamics; however it has one disadvantage not being suitable for flows with strong streamwise vorticity and has in recent developments lost ground to advantage of the $k-\omega$ model [1]. In both cases, k is the turbulent kinetic energy per unit mass. ϵ is the rate of dissipation and ω is the specific rate of dissipation. As mentioned, the $k-\omega$ has found to be the most suitable model for ship flows but there is one difficulty to be solved, it is hard to define a robust boundary equation for the ω equation at the outer edge of the boundary layer. Therefore Menter (1993) proposed that both models should be used together, the ω at the hull surface and ϵ in the free stream outside the boundary layer. In addition Menter also suggested an improved prediction of the principal shear stresses this is known as the $k-\omega$ SST model. For a deeper discussion see [17].

5.2.2 CALCULATION OF TURBULENCE COEFFICIENTS

When calculating the coefficients for the turbulence models, a trial and error methodology is used, but there are some formulas to use as a guideline. The following chapter describes how to approximate the coefficients for the $k-\omega$ and $k-\epsilon$ models with variations.

The turbulent kinetic energy k is defined as

$$k = \frac{3}{2}(UI)^2, \quad (5.3)$$

where U is the inlet velocity in m/s and I is the turbulence intensity which varies depending on the flow characteristics as,

$$I = \begin{cases} >1\% & \text{Low turbulence case; flow origins from fluid without velocity} \\ 1\% > I > 5\% & \text{Medium turbulence case; low Re flow in not so complex geometries} \\ 5\% > I > 20\% & \text{High turbulence case; high Re flow in complex geometries} \end{cases}$$

The specific dissipation rate ω is defined as

$$\omega = \frac{\sqrt{k}}{L_{turb}}, \quad (5.4)$$

where k is the turbulent kinetic energy as before and L_{turb} is the turbulent length scale which is intuitively easy to relate to the physical size of the problem. The length scale should in most cases not be greater than the dimension of the problem, which would mean that the turbulent eddies are larger than the problem size. In this case,

$$L_{turb} = 0,1H \quad (5.5)$$

where H is the height of the domain.

ϵ is calculated as,

$$\epsilon = \frac{C_\mu k^{3/2}}{L_{turb}} \quad (5.6)$$

where C_μ is a turbulence constant which usually is set to a constant value of 0.09 [18].

5.3 COURANT–FRIEDRICHS–LEWY CONDITION (CFL)

When using explicit difference schemes, to solve partial differential equations, a correct value of courant number (CFL) is essential to obtain convergence and stability of the solution. In two dimensions it is defined as

$$\frac{u_x \Delta t}{\Delta x} + \frac{u_y \Delta t}{\Delta y} \leq CFL \quad (5.7)$$

where u_x and u_y is the velocity, Δx and Δy the cell length in x - and y -direction and Δt the time step. For the condition to be fulfilled the distance that a particle travels during one time step needs to be smaller than one cell length. This means that when dealing with a high velocity and small cells the time step needs to be very small [19]. To get convergence for the simulations in this report the CFL number is kept relatively small, around 0.1.

5.4 VOLUME OF FLUID METHOD

The VOF method is used to solve for the free surface and is based on a single set of conservation equations by the use of a volume fraction variable, α . The domain Ω is in initial condition divided into two different domains where cells are defined as air or water, Ω_a and Ω_w . α is then a variable which indicates if the cell is filled with water, air or both which is the case for the free surface. It can be expressed as,

$$\alpha = \begin{cases} 1 & \text{cell filled with air, } \Omega_a \\ 0 < \alpha < 1 & \text{cell in the transition between } \Omega_a \text{ and } \Omega_w \text{ (free surface)} \\ 0 & \text{cell filled with water, } \Omega_w \end{cases}$$

The free surface is computed separated from the NS-equations and solves the transport equation,

$$\frac{\partial \alpha}{\partial t} + \frac{\partial u_i}{\partial x_i} \alpha = 0 \quad (5.8)$$

The density and viscosity is irregular in the domain and can be expressed as,

$$\rho(x, t) = \rho_w \alpha + \rho_a (1 - \alpha) \quad (5.9)$$

$$\nu(x, t) = \nu_w \alpha + \nu_a (1 - \alpha) \quad (5.10)$$

where ρ_w , ν_w is the density respectively the viscosity of water and ρ_a , ν_a is the same, but for air [20] [21].

5.5 MODELING AND NUMERICAL ERRORS

When working with CFD it is important to be aware of the existence of the numerical and modeling errors in the solution and to minimize them to get more accurate results

First, there are neglected physical effects when going from the reality to the conceptual model, where physical phenomena are identified and some are simplified or neglected. One example of this is the neglecting of flow above the free surface. The next step is to translate the conceptual model into a continuous mathematical model which includes a set of equations for solving pressure, velocity etc. To solve these equations they need to be discretized by some numerical method (i.e. finite-volume and finite-element method) which introduces discretization errors. The discretized mathematical model is solved by numerical algorithms, in most cases by iterating the solution and a criterion on the convergence of the residuals is given. When the criterion is met the iterative procedure is terminated, this introduces convergence errors. The final contribution comes from round off errors which originates from the internal representation of numbers by the computer and can affect the results more than one might expect.

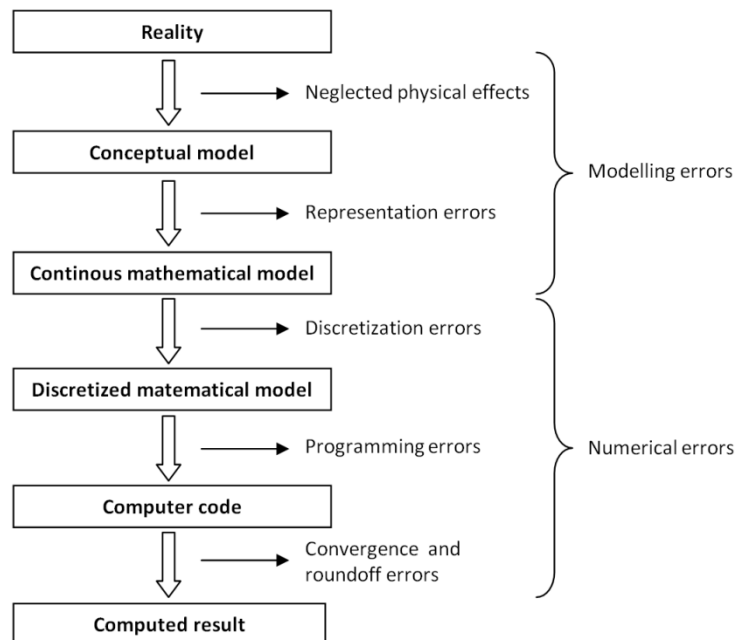


FIGURE 20. POSSIBLE SOURCE OF ERRORS IN COMPUTED RESULTS USING CFD (FROM LARSSON AND RAVEN [1])

As seen in Figure 20 the errors are often divided into two types of errors, modeling errors which are due to approximations in the conceptual and continuous mathematical models and numerical errors which come from discretization, convergence and round off errors.

There are several ways to minimize these errors, including refinement of the grid, which will make the solution converge better, ultimately to a grid-independent result. Lowering of the discretization order in the solver will make the numerical method more stable but of course less accurate [1].

5.6 MESH

The mesh is of big importance when working with CFD and there are a lot of different parameters to take into account. It is complicated trying to decide what a good mesh is, since it varies from case to case but there are some factors to be taken into account. First there should be small deviation from orthogonality, limited cell aspect ratio, smooth distribution of cell sizes, refined regions with high gradients and alignment of grid lines with the flow [1]. Further, to model the turbulence correctly, it is important to place the first grid point within a distance from the wall suitable to the chosen turbulence model. The dimensionless distance y^+ is a criteria and is defined as

$$y^+ = \frac{u_\tau y}{\nu} \quad (5.11)$$

The mesh should also be fine enough around the free surface to be able to capture it accurately. When using wall functions together with $k-\omega$ SST model the value should be in the interval $30 < y^+ < 100$ to 300 [22].

6 OPENFOAM

OpenFOAM, Open Field Operation and Manipulation, is open source software, free to use and user developed, aimed for CFD simulations and calculations. Since its open source there is a constant development of the software with more than 80 solvers and over 170 utility applications for meshing, pre and post processing. The solvers can handle almost any type of flow, for example incompressible, compressible, multiphase and combustion, both laminar and turbulent.

In this project OpenFOAM was used mainly because it is open source, i.e. free of charge, has a big community online available for questions together with knowledge at the department. It also has a flexible code with the ability to modify and many different solvers and numerical schemes to choose from. The down side is that the experience with the software were initially none, which led to a lot of time spent trying to learn how the software works. Compared to other commercial software, where all the pre and post processing is done in an intuitive GUI, it is more time demanding during the learning period since post processing is done in text files. There are a number of tutorials available which was used in an early stage to get familiar with the software.

For this project the multiphase flow solvers are of interest since it uses VOF method to solve the free surface for two incompressible or compressible fluids. The case set up in OpenFOAM is similar regardless of which solver used and consist of three main directories with folders and files; 0, constant and a system folder together with a number of optional utility folders. The constant folder contains a full description of the mesh and files specifying physical properties for the application, for example turbulence, transport and gravity. The system folder holds files and directories associated with the solution for example files defining different time parameters, discretization schemes and choice of solvers. All the initial values and boundary conditions for hydrodynamic pressure, velocity, wall functions etc. are defined in the 0 folder and a new is created for every time step solved with updated values. An example of a case setup is presented in Figure 21 [23].

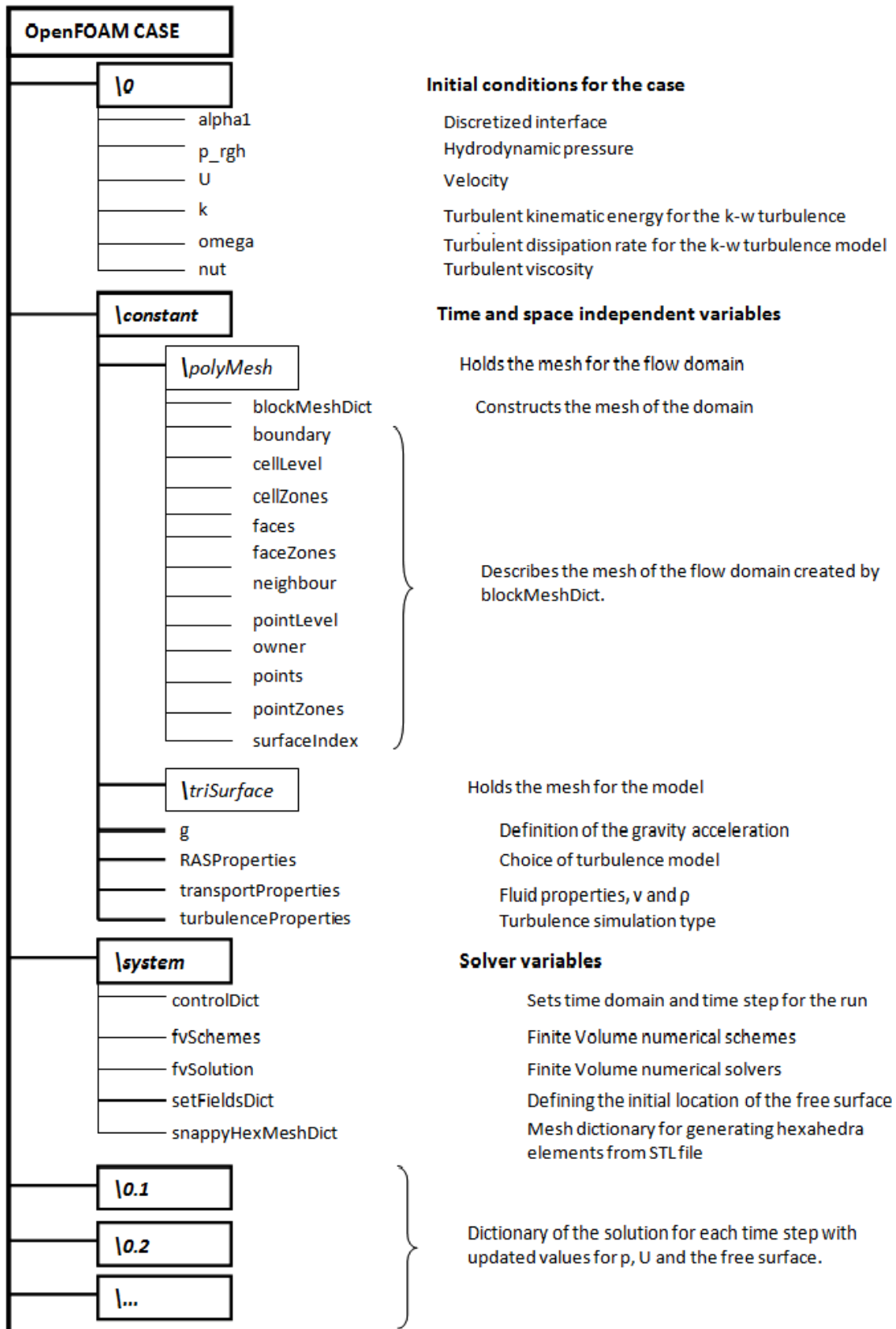


FIGURE 21. A TYPICAL CASE SET UP IN OPENFOAM WITH CASE DIRECTORIES

6.1 BOUNDARY CONDITIONS

There are three types of boundary conditions in OpenFOAM, base type which describes the type of patch in terms of geometry, i.e. patch, wall, empty, wedge or cyclic. Further on there are primitive and derived types which are used to define the condition on the basic type patches. The ones used in this thesis are:

- **zeroGradient:** Gradient of the patch field is zero.
- **fixedValue:** Normal gradient of the patch field is specified.
- **empty:** To solve for two-dimensional cases the plane normal to third dimension, where no solution is required, is set to empty.
- **totalPressure:** The total pressure is fixed and is adjusted when velocity changes
- **slip:** zeroGradient if patch field is scalar. Component normal to the patch is fixedValue zero and tangential components are zeroGradient if vector.
- **uniformFixedValue:** Used for ramping of the velocity on the inlet and outlet patches.
- **inletOutlet.** Switches velocity and pressure between fixedValue and zeroGradient depending on direction of velocity.

Different wall function are also available in OpenFOAM, that is used as boundary conditions on patches and are defined in a separate file, here omegaWallFunction, nutkWallFunction and kqRWallFunction is used for the $k-\omega$ SST model. For more information see OpenFOAM User Manual [23].

6.2 UTILITIES AND SOLVERS

In this chapter the utilities used in the project are presented. For more information see OpenFOAM User Manual [23].

6.2.1 BLOCKMESH

The blockMesh utility creates parametric meshes with optional grading and curved edges. The idea with blockMesh is to represent the domain with one or more three-dimensional, hexahedral blocks. In turn, the blocks are described by a number of vertices in each corner of the blocks.

6.2.2 CHECKMESH

A utility to check the mesh for validity based on patch topology for connected surfaces. The most common errors are:

- **Skewness:** Disagreement between shape of a cell in grid and an equilateral cell that has same volume which leads to inaccurate solutions.
- **Non-orthogonality:** If the angles between cells deviate too much from the optimal value, i.e. 90° or 60° for quad and triangular elements respectively, discretization errors will occur and a diverged solution.
- **Aspect ratio:** When the relation between cell height and length gets to large it leads to round-off errors and convergence problems.

It also gives the user statistics for the mesh such as number and type of cells, points, faces and the topology for multiply connected surfaces and is an important tool to see the quality of the mesh [20] [23].

6.2.3 SETFIELDS

The setFields dictionary is used to divide the calculation domain into two types of fluid, with different density and viscosity. It uses a phase fraction parameter α according to the VOF method and defines a box where alpha equals one. In this case water and the parts outside is set to air, i.e. α equals zero.

6.3 INTERFOAM

interFoam is a solver to be used in OpenFOAM when dealing with two incompressible, isothermal and immiscible fluids. The solver uses VOF phase-fraction to capture the interface between the fluids. It requires a very good mesh and low time stepping to calculate pressure fields or it becomes very unstable [20].

6.4 NUMERICAL SCHEMES (FVSCHEMES)

The choice of discretization schemes is defined in the fvSchemes file and has a large influence on whether the solution converges or not. Input variables related to the finite volume numerical schemes ranges from derivatives, gradients to interpolation of values from one set of points to another.

OpenFOAM gives the user complete freedom to choose from different interpolation schemes for all interpolation terms. In Table 1 below the different set of terms, for which numerical schemes are specified, are listed.

TABLE 1. TERMS FOR THE NUMERICAL SCHEMES USED IN OPENFOAM

Numerical scheme	Description
ddtSchemes	Time derivatives
interpolationSchemes	Point-to-point interpolations of values
snGradSchemes	Component of gradient normal to a cell face
gradSchemes	Gradient ∇
laplacianSchemes	Laplacian ∇^2
divSchemes	Divergence $\nabla \cdot$
fluxRequired	Fields which require the generation of a flux

The time derivatives are specified in the ddtSchemes sub-dictionary. The schemes can be explicit or implicit numerical schemes where explicit means the solution for current time step is computed from known previous solutions. Implicit schemes means the solution is evaluated both from the unknown current and previous time step and has to be solved iteratively.

The interpolation schemes contains the terms handling the interpolation of values, typically from the center of the cell to the center of the faces. Surface normal gradient terms are stored in the snGradSchemes which is evaluated at a cell face, the component normal to the face. It can be i.e. corrected, uncorrected, limited which means explicit, none or limited non-orthogonal correction. The gradSchemes includes the gradient terms of the solution while the laplacianSchemes the Laplacian terms. Further on, divSchemes contains the divergence terms for example $\nabla \cdot (\rho UU)$ which is a term in the momentum equation and is given in OpenFOAM format as *div(phi, U)* where *phi* refers to flux, $\phi = \rho U$. The only choice the user has for the discretization scheme is gaussian scheme together with various interpolation schemes.

The fluxRequired which describes which equation is solved for generating the flux, for example pressure, which is the case in most fluid dynamic problems. A more extensive explanation can be found in the OpenFOAM manual [23].

6.5 SOLUTION ALGORITHM CONTROL (fvSOLUTION)

The equation solvers, algorithms and tolerances on the residuals are controlled in the fvSolution dictionary. The solvers are iterative and to control the solution tolerances on the residuals are set. The solver will then iterate until the given criterion is fulfilled. Another option is to define the maximum number of iterations desired. Before running a solver, preconditioners might be used in order to decrease the numbers of iterations needed [24]. The preconditioners available are listed in Table 2:

TABLE 2. THE DIFFERENT PRECONDITIONERS AVAILABLE IN OPENFOAM

Preconditioner	Keyword
Diagonal incomplete-Cholesky (symmetric)	DIC
Faster diagonal incomplete-Cholesky (DIC with caching)	FDIC
Diagonal incomplete-LU (asymmetric)	DILU
Diagonal	diagonal
Geometric-algebraic multi-grid	GAMG
No preconditioning	none

Further, when solving the Navier-Stokes equations one is dependent on the pressure through the pressure gradient in the momentum equation but the pressure lacks its own equation. This can be solved by transforming the continuity equation into an equation for the pressure. One will end up with two non-linear equations, one for the pressure and one for the momentum. This is what is done in the SIMPLE (Semi-Implicit Method for Pressure-Linked Equations) and PISO (Pressure Implicit with Splitting of Operators) algorithms. The first is used for steady state flow whereas the latter is used for transient flow. For a deeper discussion about SIMPLE and PISO see [25]. Finally, PIMPLE is a merged version of the two which uses under-relaxation with multiple momentum correctors and is good for transient solution of NS with lower restriction on the maximum courant number [26].

7 CASE SET UP

7.1 AIM WITH THE STUDY

The aim with a two-dimensional case is to investigate the possibility to perform a fast and simple simulation to gain knowledge on how the basic geometry of the moonpool is affecting the characteristics of the flow. Also, if there are any trends to be identified on the resistance when changing parameters such as moonpool length, draught and recess height. The results are to be compared with known model test data for validation.

7.2 PHYSICAL MODELS

To model the flow in the moonpool accurately, the turbulence and the interaction between the two phases, water and air needs to be modeled. The turbulence is modeled by using the $k-\omega$ SST model mainly because in literature this is the model recommended for this type of flow problem since it combines the $k-\omega$ and $k-\epsilon$ model [1]. VOF phase-fraction is used to simulate the free surface by dividing the domain into two mediums with different viscosity and density. Both models and the VOF method are further discussed in Chapter 5.

7.3 GEOMETRY

As mentioned above, the focus of this study is the behavior of the flow in the moonpool. The geometry is simplified to a two-dimensional case, based on the reference case from SHI [6] and the simplest geometry is a square moonpool with vertical walls, as seen in Figure 22. To see how the flow behavior is affected by different geometry changes two more types of moonpools have been set up with a recess in the aft and in both front and aft. These are compared with test data from model test conducted by SHI [6]. For all the cases the recess height, R_H , has been changed while the length, R_L , is kept constant.

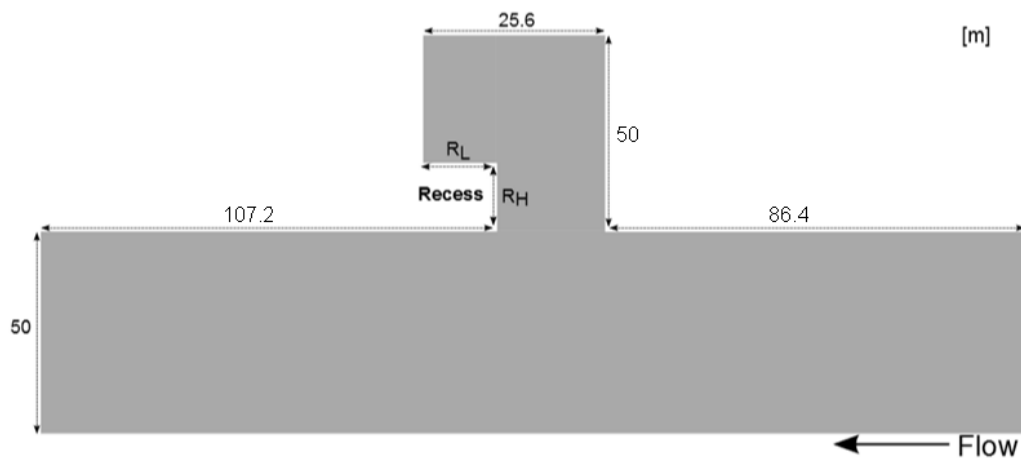


FIGURE 22. GEOMETRY WITH DIMENSIONS WITH VARIABLE LENGTHS R_H AND R_L FOR THE RECESS

The dimensions of the domain are kept constant where L_{pp} is 207.2 m, the height below the hull is 50 m and a moonpool height of 50 m. The domain is one cell wide in the z -direction with the length of 1 m, this is because OpenFOAM require a three-dimensional domain. The dimensions are scaled by a factor of 0.041 to match the dimensions from the model tests.

7.3.1 REFERENCE CASE DIMENSIONS (SHI)

TABLE 3. REFERENCE CASE DIMENSIONS WITH NAMES

Name	Recess type	R _H [m]
S0	No recess	-
S1	Original recess	7.3
S2	High recess	8.15
S3	Low recess	6.45
S4	S1 with Forward recess	7.3

7.4 BOUNDARY CONDITIONS

As seen in Figure 23 the boundaries to be defined are patches at the inlet and outlet, walls representing moonpool, top, bottom and sides of the domain. In OpenFOAM the domain is defined in three dimensions therefore in a two-dimensional case the third dimension has to be neglected and the walls perpendicular to the z-direction, *frontAndBack*, are set to empty.

At the *inlet* a velocity is defined by a fixed value which is initially zero and then ramped, i.e. accelerated to a desired value. The reason for this is to get a smooth transition for the velocity; otherwise there are large velocity fluctuations initially in the moonpool and the solution might not converge. The pressure at the *inlet* is defined as *bouyantPressure* with value 0, this according to recommendations found in the user guide [23]. At the *outlet* the purpose is that the fluid should exit the domain without affecting the flow, the velocity is then a *zeroGradient* boundary condition and pressure is same as the *inlet*, *bouyantPressure* with value 0. At first there was an *atmosphere* patch on the top of the moonpool with a *totalPressure* boundary condition but this gave problems with the solution, with pressure and velocity fluctuations and demanded a forced flow *outlet*. In the final set up the top wall of the domain is a wall with a *fixedValue* uniform 0 for velocity and *zeroGradient* for pressure. The same boundary conditions for velocity and pressure is set to the *fixedWalls* patches, representing the hull bottom, since the velocity on a wall which is not slip has a zero velocity because of the boundary layer creation. The *bottom* patch should not interfere with the solution and is set to a *slip* condition. The pressure mentioned above is referred to the hydrodynamic pressure. For explanations of the different boundary conditions see Chapter 6.1.1 and the different boundary conditions are summarized in Table 4.

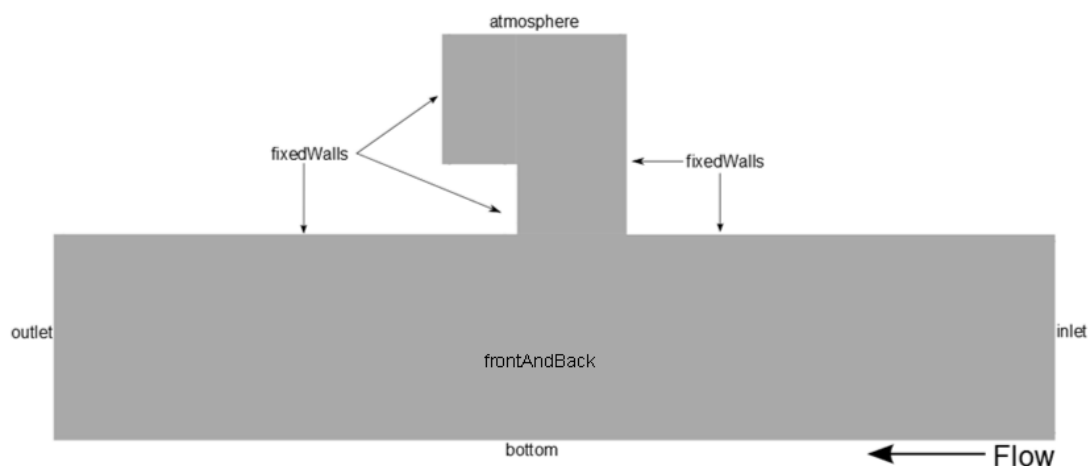
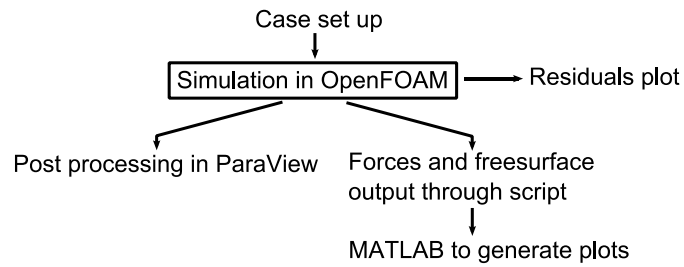


FIGURE 23. PATCHES FOR THE SQUARE MOONPOOL WITHOUT MODIFICATIONS

TABLE 4. BOUNDARIES IN THE PROBLEM AND THE INITIAL BOUNDARY CONDITIONS.

Boundary	U	P_rgh	k	Omega
Inlet	uniformedFixedValue	bouyantPressure	fixedValue	fixedValue
fixedWalls	fixedValue	zeroGradient	kqRWallFunction	omegaWallFunction
Outlet	zeroGradient	bouyantPressure	zeroGradient	zeroGradient
Top	fixedValue	zeroGradient	inletOutlet	inletOutlet
Bottom	slip	zeroGradient	kqRWallFunction	omegaWallFunction
frontAndBack	empty	empty	empty	Empty

7.5 FLOW CHART



The flow chart shows the work order, from case set up to the results obtained. The post processing from OpenFOAM has been both through the software *ParaView*, which is included in OpenFOAM and MATLAB, a scientific computing program. The forces are given, for patches defined by the user during the pre processing, where the pressure and viscous forces are added in the x-direction to give the total resistance component.

7.6 MESH

The final mesh for the reference case with the aft part moonpool is presented in Figure 24 and this mesh setup was used for all the different cases, with varying number of cells in the y -direction of the moonpool, depending on the recess height. In the area of the moonpool there is a lot of circulation of the flow and also the presence of the free surface, which leads to high requirements on the quality of the mesh. The same goes for the area in the free stream close to the wall because of the boundary layer creation together with the representation of the turbulence and separation point. To get the correct representation without the need for the adding of too many cells, the mesh is stretched in the x - and y -direction.

To find the optimal grid, which captures the turbulence accurate enough, a turbulence validation were carried out on a flat plate and compared to a theoretical value for the drag coefficient (C_D), see Chapter 7.6.1. The y^+ value for the final mesh is around 40 which is within the required range according to Chapter 5.6. The distance from the wall in the flow domain is around 1 mm and 4 mm for the walls inside of the moonpool. It should really be pointed out that in the early stages of the project there were a lot of problems with the mesh, which gave unphysical results. This led to a lot of time spent on improving the mesh together with boundary conditions, but still having reasonable calculation times.

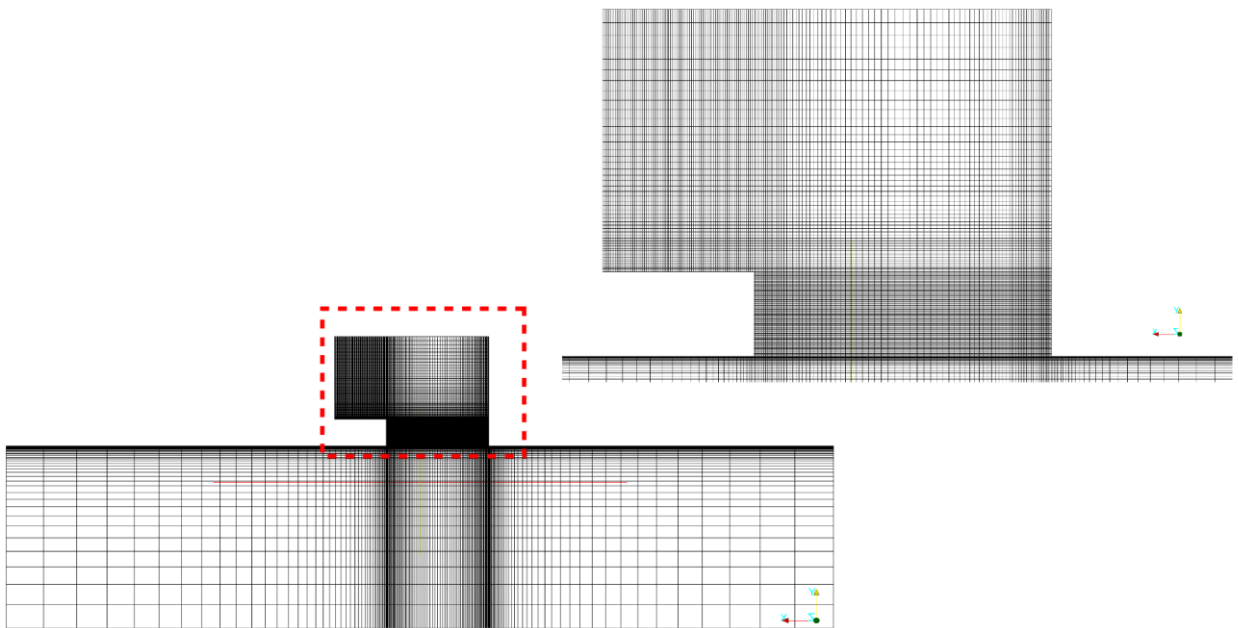


FIGURE 24. MESH FOR THE SIMULATIONS OF THE REFERENCE CASE S1

7.6.1 TURBULENCE AND MESH VALIDATION

This is mainly a tool to optimize the mesh for calculation time but still get accurate results from the turbulence model chosen together with boundary conditions. This is an important step when there is a limited amount of computing resources available, which sets a limit on number of cells in the mesh. The study is set up for a calculation domain without the moonpool present, i.e. a flat plate. The variable that is compared for the different cases is the drag coefficient, which is compared with a theoretical value calculated as,

$$C_D = 0.074(R_e)_x^{-\frac{1}{5}} \tag{7.1}$$

where

$$(R_e)_x = \frac{\rho u_0 L}{\mu} = \frac{u_0 L}{\nu} = 3.835 \cdot 10^7. \tag{7.2}$$

This gives a theoretical value equal to 0.023 of C_D for the flat plate.

TABLE 5. THE DIFFERENT CASES FOR THE GRID DEPENDENCY STUDY

Case	Cells, X-dir	Cells, Y-dir	No. of Cells	y+	Stretch
G1	100	40	4000	40	0.0014
G2	40	40	1600	100	0.0041
G3	40	40	1600	200	0.00958
G4	320	40	12800	200	0.00958
G5	40	40	1600	500	0.0309
G6	400	40	16000	40	0.0014
G7	1000	40	40000	40	0.0014

As seen in Figure 25 the value of C_D converges towards a value near the theoretical for all the grids but for the case G5, G6 and G7 the difference is about 0.40% from the theoretical value which is acceptable. Compared to the limits on $y+$ from the theory the cases G6 and G7 are preferred over G5. Since both of the cases have the same $y+$, but case G6 has less cells and less computing time this is the one preferred for the simulations of the moonpool.

TABLE 6. DIFFERENCE FROM THEORETICAL VALUE FOR CASE G1-G7

Case	C_D	Difference from theoretical value
Theoretical	0.002252	0%
G1	0.002265	0.610%
G2	0.002301	2.210%
G3	0.00230	2.170%
G4	0.002284	1.450%
G5	0.002262	0.447%
G6	0.002259	0.325%
G7	0.002259	0.325%

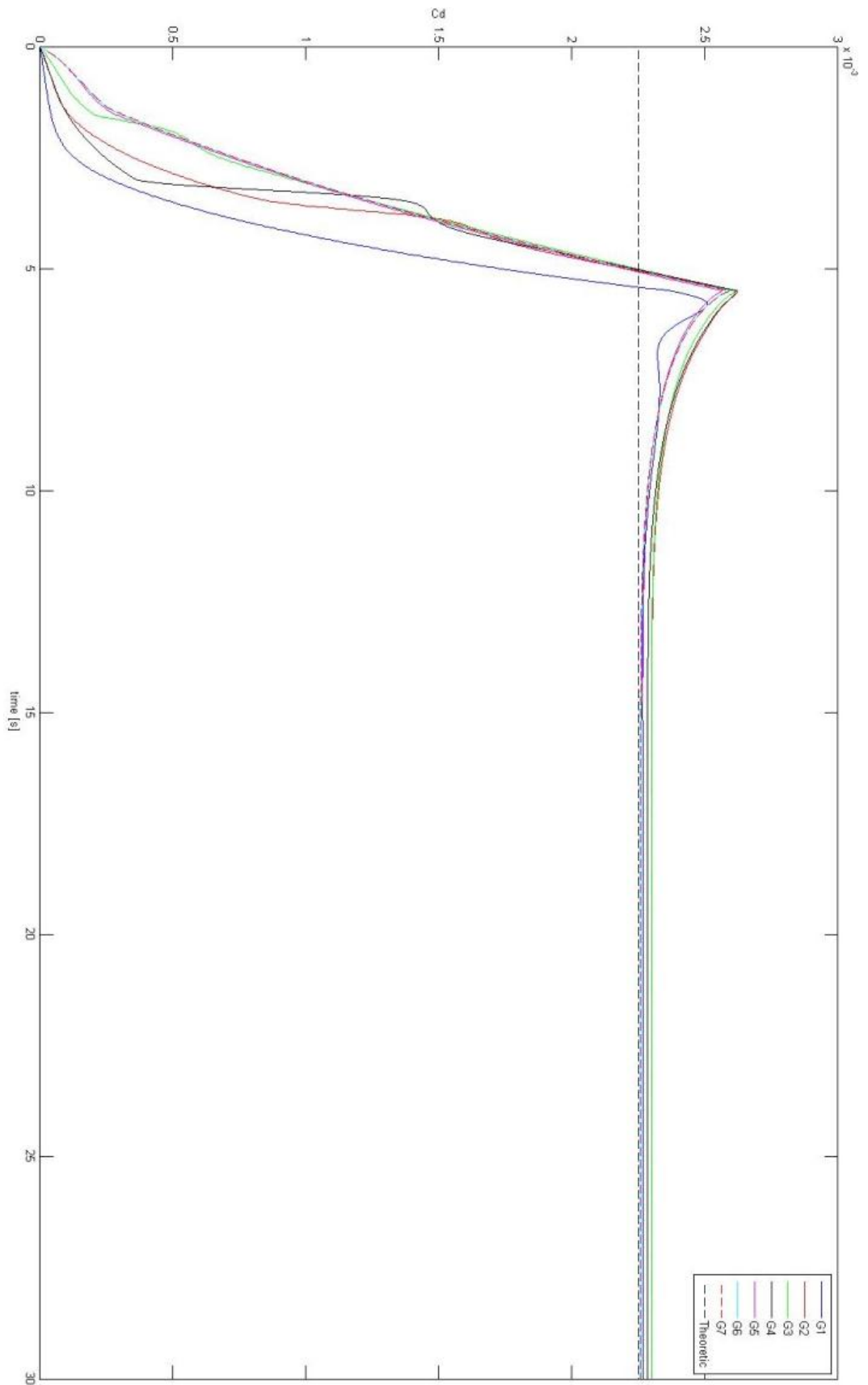


FIGURE 25. COMPARISON OF C_D VALUES FOR DIFFERENT GRIDS

8 RESULTS AND DISCUSSION

In this study the flow in a moonpool has been analyzed with respect to the flow field behavior and the drag changes due to geometry changes of the moonpool.

8.1 FLOW FIELD BEHAVIOUR

For the case with a rectangular moonpool without recess, S0, the sloshing natural period of the free surface oscillations from the simulations can be validated with an analytical solution of a rectangular tank with a free surface. The analytical solution is given by

$$T_N = \frac{2l}{(gh)^{1/2}} \quad (8.1)$$

where h is the height of the free surface inside the tank and l is the length of the tank [27]. T_N is equal to 1.126 s for a moonpool with the dimensions from case S0.

The movement of the free surface is initiated by a vortex created at the forward edge by separation of the shear layer when the surface, which maxima are at the downstream wall a new vortex is created, Figure 24. The new vortex is then built up as the free surface moves towards the upstream wall, Figure 25. This build up is continuing until the surface maxima is at the upstream wall and then is returning back, Figure 26. The vortex is then shed and starts to travel downstream. This process is periodic and it has been observed that the vortex is shedding at the same period as the free surface oscillations, calculated with Equation 8.1.

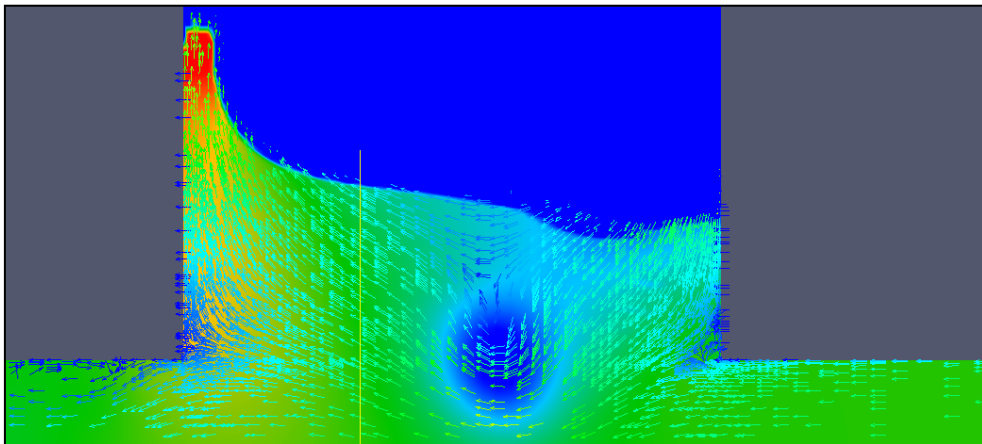


FIGURE 26. INITIATION OF THE VORTEX AT THE FORWARD WALL (VECTORS REPRESENT VELOCITY, BACKGROUND PRESSURE)

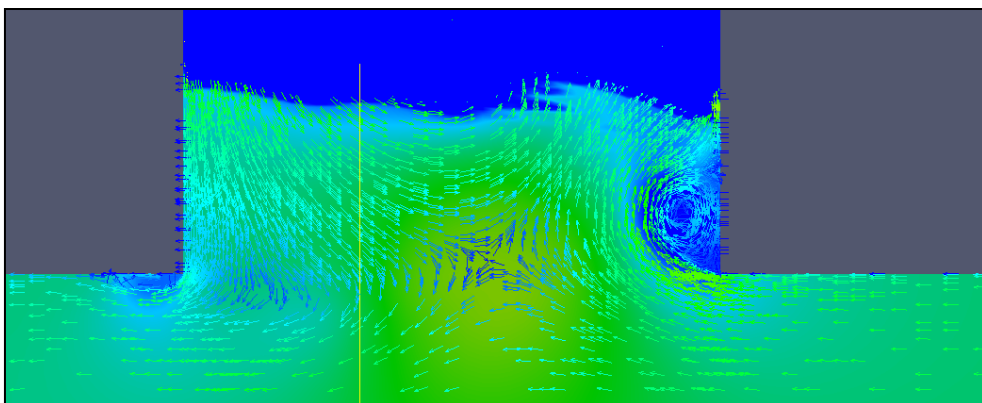


FIGURE 27. VORTEX BUILD UP

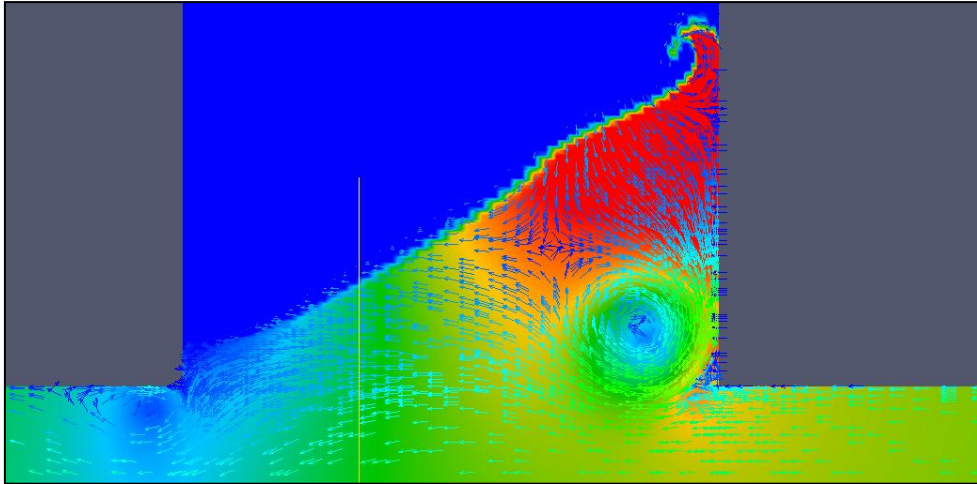


FIGURE 28. VORTEX AND FREE SURFACE ELEVATION AT ITS MAXIMUM BEFORE SHEDDING

In Figure 29 to Figure 35, a CFD simulation of a sequence describing the flow behavior in the moonpool is shown, for the reference case S1 where the velocity field is represented by vectors and in the background, the variation in dynamic pressure. Blue represents low velocity respectively low pressure and red is high.

As in case S0, the flow field behavior and free surface motion is initiated due to a boundary layer built up at the wall upstream the moonpool. The leading edge of the moonpool decelerates the flow since it causes a loss in energy and the boundary layer flow is unable to follow the sharp corner, Figure 29. As a result, separation will occur and a recirculation area will be created at forward wall of the moonpool. This area will be fed with fluid from the boundary layer until it grows so large that energy, in form of a vortex, has to be shed, Figure 30. The vortices will shed at a certain frequency and travel downstream until it reaches the aft wall and redirects flow which enters the moonpool. As the vortex approaches the downstream wall the pressure on the wall increases, Figure 31. The wall forces the flow to change direction and a main part of the flow goes upward and elevates the free surface, Figure 33. This results in a continuous process leading to oscillations of the free surface and as the old vortex is leaving the moonpool a new one is initiated, Figure 34.

The flow pattern is similar to S1 for the cases S2 and S3 but has different amplitude of the free surface elevations. By varying the height of the recess, the amount of flow allowed to enter above the recess is varied. In Appendix I the flow pattern for minimum and maximum drag and pressure is presented for the cases S0-S3. Comparing the cases with moonpool (S1, S2, S3) to the one without (S0) it can be seen that the flow is changed as a recess is introduced. The biggest change is that the flow instead of going directly back to the moonpool is dampened out above the recess. This causes the motions to be less violent. In addition, the free surface elevation and the resistance decrease.

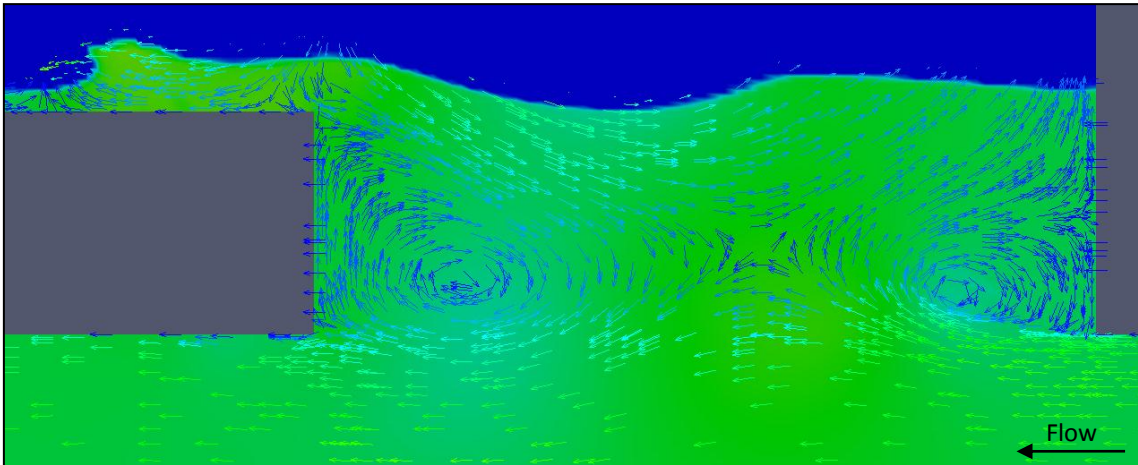


FIGURE 29. INITIATION OF VORTEX AT LEADING EDGE, CASE S1

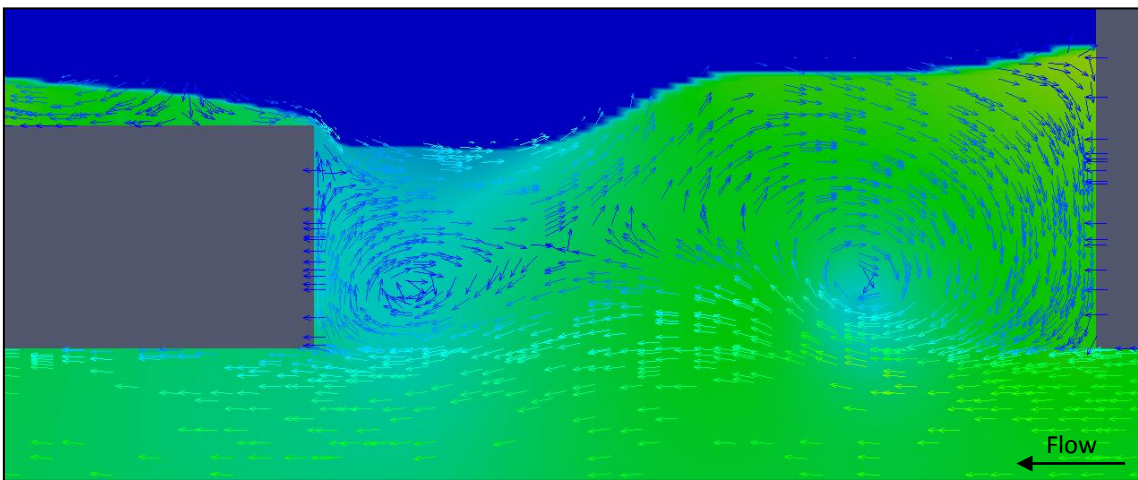


FIGURE 30. VORTEX SHED AND TRAVELS DOWNSTREAM

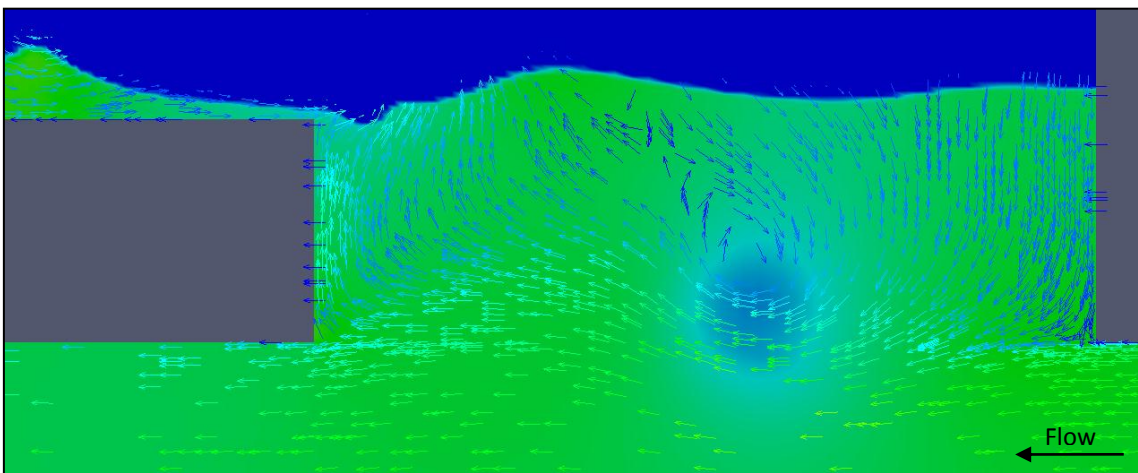


FIGURE 31. TRAVEL DOWNSTREAM AND REDIRECTS FLOW WHICH ENTERS MOONPOOL

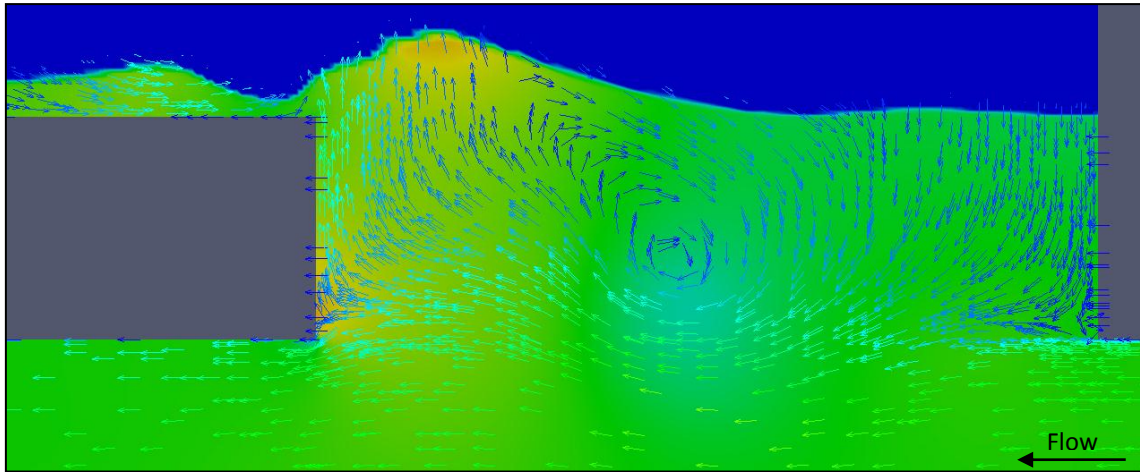


FIGURE 32. PRESSURE ON THE AFT WALL INCREASES AS MORE FLOW IS REDIRECTED UP INTO THE MOONPOOL

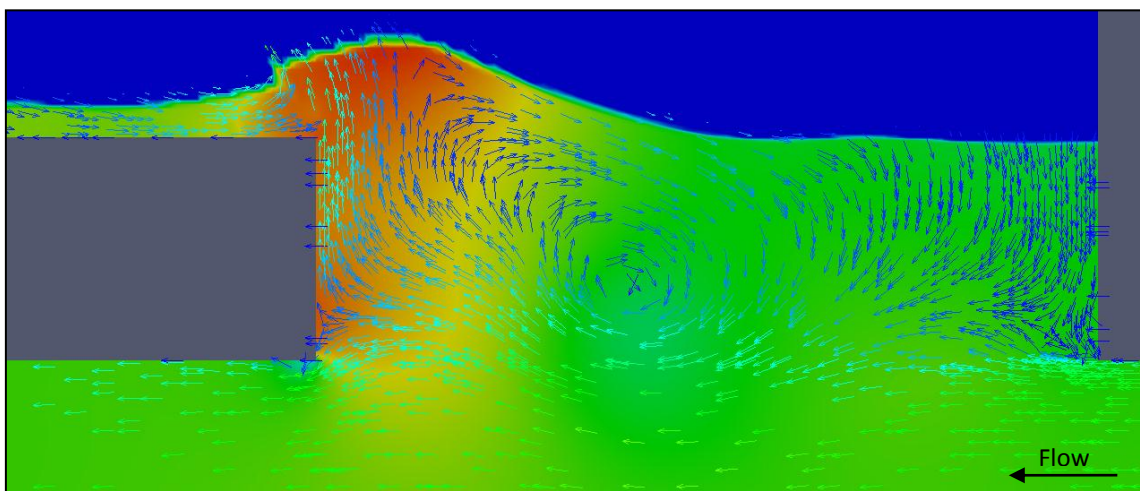


FIGURE 33. PRESSURE MAXIMA, FLOW IS DIRECTED UPWARDS BY THE WALL AND ELEVATES THE FREE SURFACE

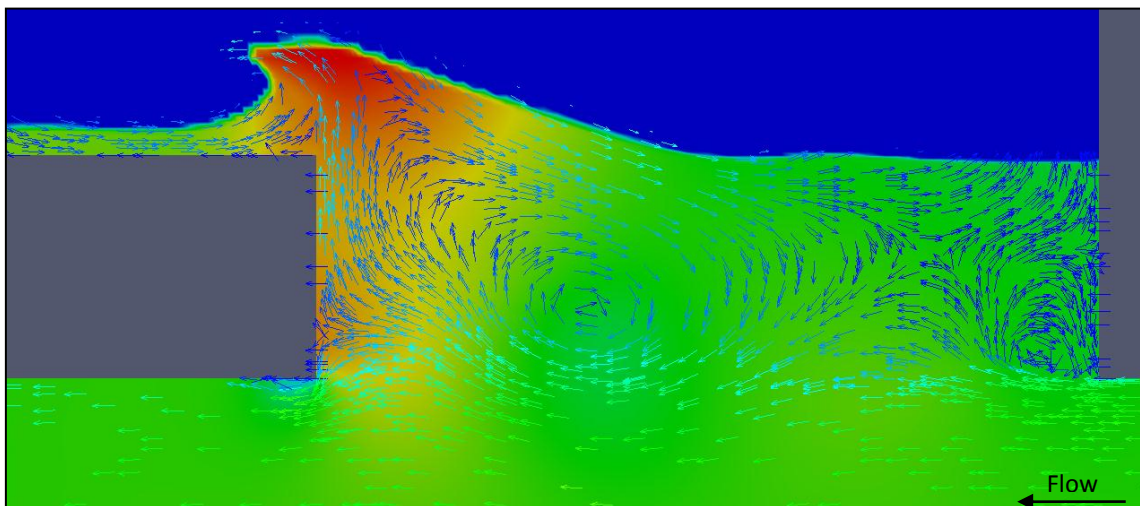


FIGURE 34. BREAKING OF THE FREESURFACE AND THE INITIATION OF A NEW VORTEX AT LEADING EDGE

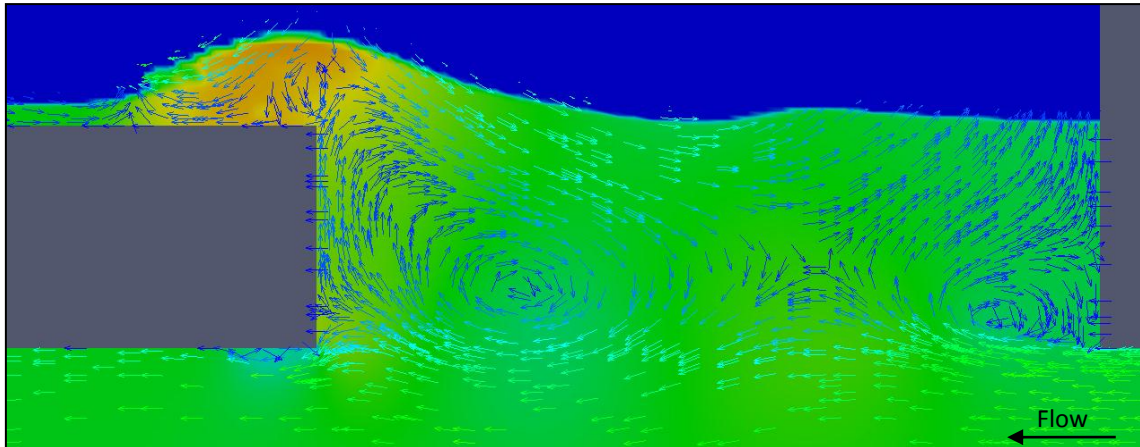


FIGURE 35. COMPLETION OF THE FULL SEQUENCE

In the case with both forward and aft recess, S4, only an initial vortex is created and becomes stationary in the aft part of the moonpool. Hence, the oscillations of the free surface are not triggered by continues vortices and the motion is very small compared with the other cases. This is thought to be because of a geometrical coincidence with the dimensions of the forward and aft recess height and the draught in S4. The results are shown in Figure 36. However, it was shown that by varying the recess length or height the creation of continues vortices at the forward edge are initiated, shown in Figure 37.

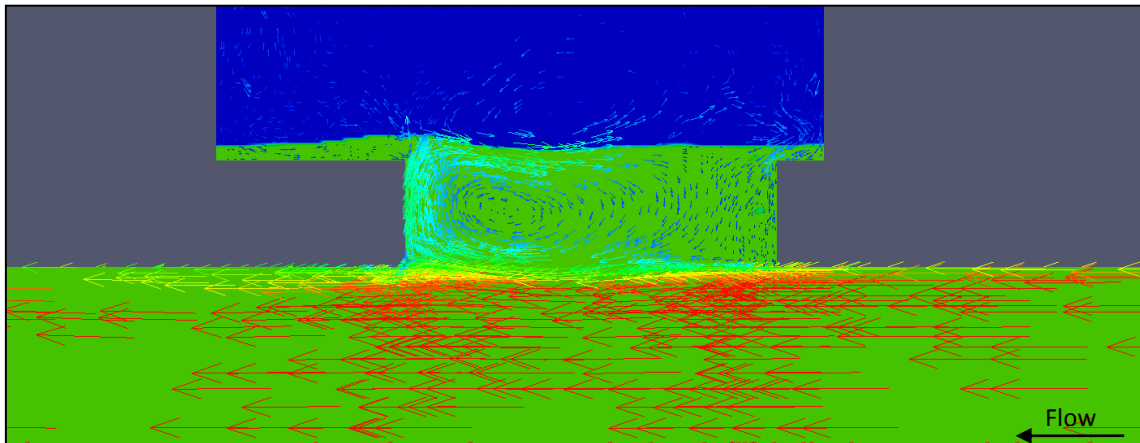


FIGURE 36. FLOW PATTERN FOR CASE S4 WITH NO WORTEX CREATION AT FORWARD WALL

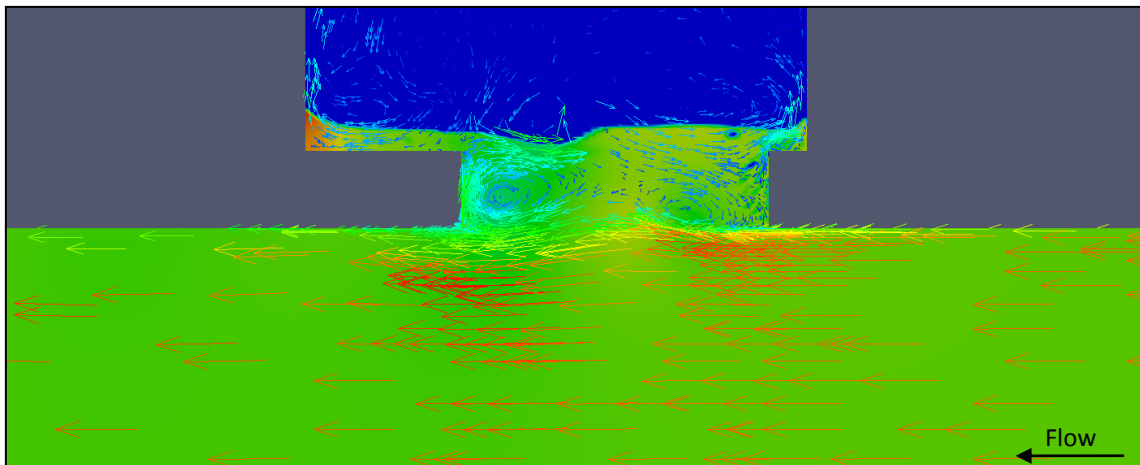


FIGURE 37. FLOW PATTERN FOR CASE S4 WITH LOWERED RECESS HEIGHT

An attempt was made on a three dimensional simulation where the domain from the case S1 was extruded 12 m in the third direction. After four days of running on 32 processors the simulations were stopped since only 23 seconds of the simulation had been calculated and the drag curve had not converged. However, some effects, previously mentioned as 3D effects, could be seen, Figure 38. Two vortices are created at the moonpool sides and the free surface starts to move in all three dimensions.

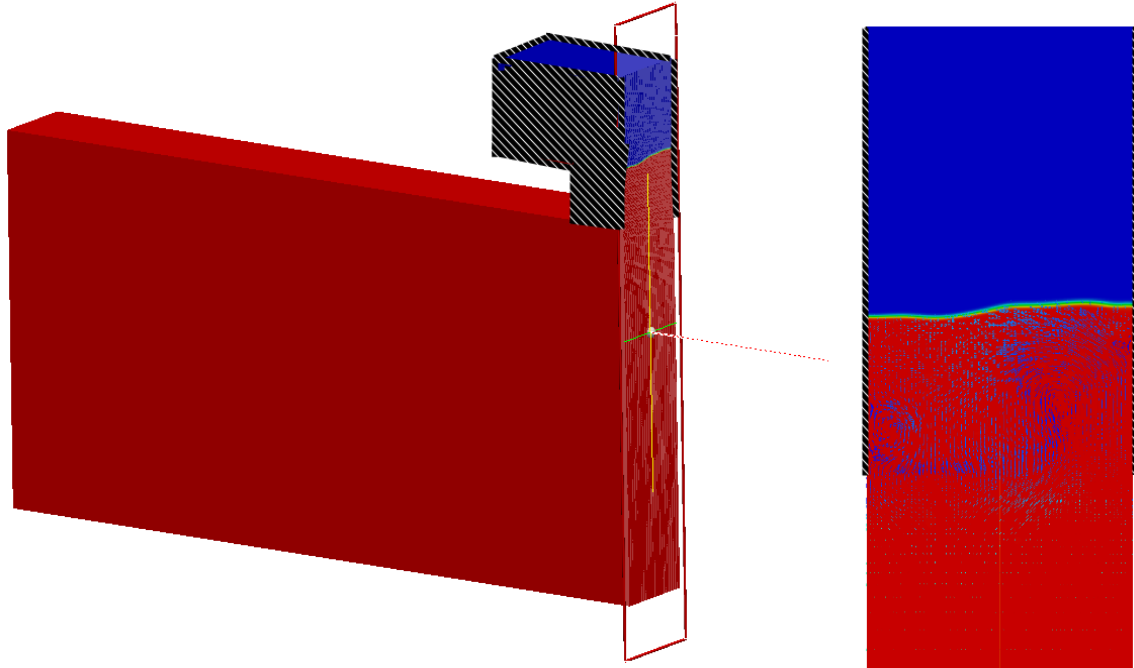


FIGURE 38. FLOW FIELD SIMULATED IN THREE DIMENSIONS FROM CASE S1

8.2 EVALUATION OF DRAG

In the reference case the EHP saving for the different set ups are presented. S1 is used as a reference when comparing the differences between them. A trend has been shown, seen in Table 7 below. The data is based on model tests performed by SHI [6].

TABLE 7. RESULTS FROM MODEL TESTS PERFORMED (FROM SHI [6])

Name	Recess type	R _H [m]	EHP saving
S0	Normal rectangular without recess	-	-3%
S1	Original recess	7.3	0%
S2	High recess	8.15	9%
S3	Low recess	6.45	-1%
S4	S1 with Forward recess	7.3	7%

An attempt was made to reproduce the trends on the drag from the model test with two dimensional CFD simulations. The variable that was compared was the total drag, computed by an algorithm in OpenFOAM, on the fixed walls and the result is shown in Table 8.

TABLE 8. RESULTS FROM TWO-DIMENSIONAL CFD SIMULATIONS

Name	Recess type	R _H [m]	Total drag saving
S0	Normal rectangular without recess	-	-59%
S1	Original recess	7.3	0%
S2	High recess	8.15	14%
S3	Low recess	6.45	9%
S4	S1 with Forward recess	7.3	63%
S5	S4 with lowered recess	6.45	32%

The results indicated that there can be savings made by introducing a recess type moonpool. However, two-dimensional simulations are not sufficient to compare the relatively small difference in resistance when changing the moonpool recess height. The reason for this could be that three-dimensional effects are neglected. There are small changes between the cases S0-S4 and a small part of the deviation of the CFD results could be because of numerical errors.

In Figure 39 the total drag force in the x-direction is plotted and the convergence of the solution can be seen. The period of the oscillations is directly correlated with the movement of the free surface.

In Figure 40 a comparison between the cases S4 and S5 is presented. It is shown in previous chapter that changing the height of the recess for case S4 changes the flow behavior. This leads to changes in the resistance, where S5 gives a more realistic result compared to the rather small oscillations in S4.

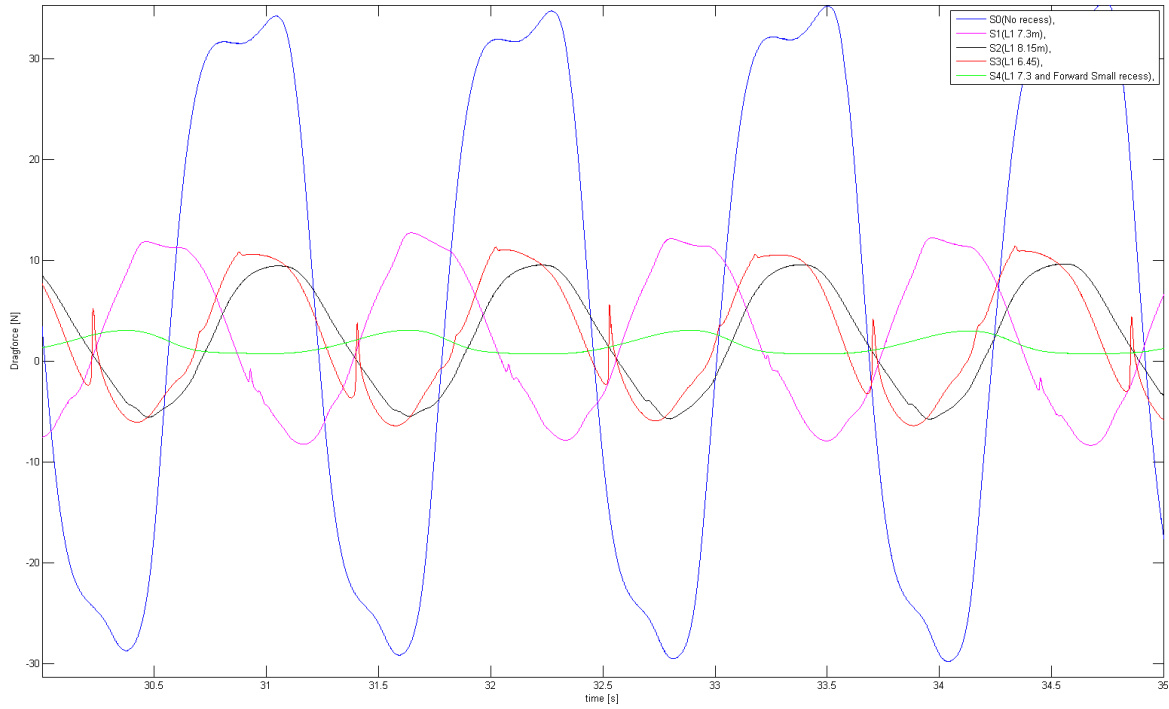


FIGURE 39. DRAG FORCE COMPARISON FOR THE DIFFERENT CASES S0-S4 (NUMERICAL SIMULATION)

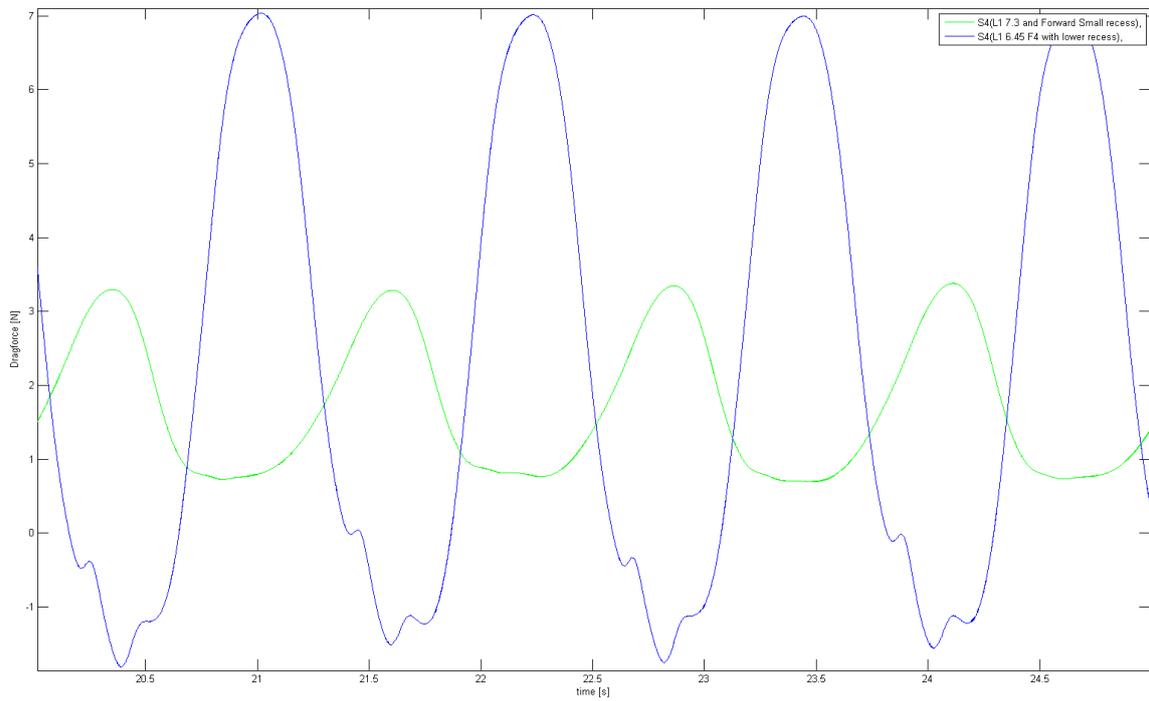


FIGURE 40. THE DIFFERENCE IN DRAG FORCE BETWEEN CASE S4 AND S5 (NUMERICAL SIMULATION)

9 CONCLUSIONS

In this thesis the flow behavior in a moonpool of a drillship has been investigated numerically, by the use of OpenFOAM which is an open source software aimed for solving CFD problems. The flow for this case is very complicated and includes both strong vortices together with a free surface.

There are two situations leading to an increase in motion of the water in the moonpool, the first one is due to the ships forward speed and the second is waves approaching the ship in operating condition. The reason for the increased movement is the oscillation of the free surface, in either sloshing (surge) or piston (heave) direction. The reason for the movement is separation of the shear layer at the forward edge of the moonpool, creating strong vortices that travel up the trailing edge and interacts with the free surface. There are two possible solutions trying to avoid this, first one is trying to avoid vortex creation and the second one is to reduce the water column oscillations by damping. This has been subject for several studies in the past, which has been used as a base for this work. Several successful solutions have been developed, some of them protected by patents.

During the project, it has been noticed that a good mesh is of great importance. Diverging solution and strange appearances of the flow, with pressure and velocity fluctuations were seen and could be eliminated by improving the mesh. The mesh has been evaluated for a simple case of a flat plate in order to capture the turbulence correctly. Limitations of computer resources led to a limit on the mesh resolution and that the focus of the project was to simulate the flow in two dimensions.

To validate the simulations of the flow in the moonpool a report from SHI [6] has been used which presents results for model tests of different recess moonpools. In addition the oscillation period has been compared between the numerical solution and a value calculated analytically. It was not possible to reproduce the trends on resistance shown in the SHI report and it is not enough to use two-dimensional CFD simulations to evaluate different moonpool designs. However, the flow pattern has been successfully simulated and this can be used to get a deeper understanding of the flow phenomena and how to reduce the oscillations.

Finally, in the end of the project the two dimensional case was extruded in the third direction and although the simulations did not run long enough to make the drag converge it was possible to get some indication on the three dimensional effects. Vortex creations at the moonpool sides could be observed but further investigations is needed to understand the complex behavior better.

10 FURTHER WORK

Since this work has a fixed velocity and also only varying the recess height it would be of interest to see how changes in the velocity would impact the water column movement in the moonpool and how varying recess length changes the damping. It would also be interesting to change the draught, since it has been kept constant throughout the work and see how it affects frequency and amplitude of the free surface oscillations.

Finally, with more computational resources, it would be of great interest trying to find a cost effective method to simulate three dimensional cases to evaluate three dimensional effects and to be able to evaluate the drag.

BIBLIOGRAPHY

- [1] L. Larsson and H. C. Raven, *The Principles of Naval Architecture Series; Ship resistance and flow*, The Society of Naval Architects and Marine Engineers, 2010.
- [2] G. Gaillarde and A. Cotteleer, "Water motion in moonpools empirical and theoretical approach," Maritime Research Institute Netherlands (MARIN), HMC Heerema, 2005.
- [3] S. Sadiq and Y. Xiong-liang, "Multi-Dimensional Numerical Free Surface VOF Modeling with Moon Pool Experiments," in *Proceedings of the ASME 27th International Conference on Offshore Mechanics and Arctic Engineering*, Estoril, 2008.
- [4] B. Molin, "On the piston and sloshing modes in moonpools," in *J.Fluid Mech*, vol. 430, 2000.
- [5] R. van 't Veer and H. J. Tholen, "Added resistance of moonpools in calm water," in *OMAE200857246*, Estoril, Portugal, 2008.
- [6] S. Hye-Jong, K. Man-Whan, C. Soon-Ho and H. Seung-Myun, "Drag reduction of recess type moonpool under vessel's forward speed," Estoril, Portugal, 2008.
- [7] J. J. Park, S. M. Kim, S. H. Lee, K. Y. Ahn, B. Y. Kim and K. M. Ha, "Development of Design Technologies for Optimum Moonpool Shapes of Drill Ships," ASME, San Diego, 2007.
- [8] K. Fukuda and Y. Yoshii, "Flow Calculations in Vertical Cavity with Free Surface and Bottom Opening to Water Surface," *The Journal of the Japan Society of Naval Architects and Ocean engineer*, vol. 10, pp. 23-28, 2009.
- [9] J. W. English, "A means of reducing the oscillations in drillwells caused by vessel's forward speed," in *The Naval Architect*, 1976, pp. 88-90.
- [10] A. Aalbers, "The water motions in a moonpool," *Ocean Engineering*, Vol 11, No 6, 1984, 1984.
- [11] K. Fukuda, "Behaviour of water in vertical well with bottom openings of ship, and its effect on ship motions," *Journal of the Society of Naval Architects of Japan*, pp. Vol. 141, pp 107-122, 1977.
- [12] CAS, "American Chemical Society," [Online]. Available: <http://www.cas.org/expertise/cascontent/caplus/patcoverage/patkind.html>. [Accessed 11 May 2012].
- [13] H.-J. Son and K. Su-Hyung, "Moonpool and drillship having the same". United States of America Patent US0197802, 2011.
- [14] A. Young-Kyu, K. Hong-Su, K. Seong-Soo and P. Jong-Jin, "Anti-sloshing decice in moonpool". United States of America Patent US7918174, 2011.
- [15] S. In-Hwan and C. Young-Bok, "Resistance reducing device for a moonpool". Europe Patent EP2374708, 2010.
- [16] W. P. Nuss, "Bouyant moonpool plug". United States of America Patent US6503022, 2003.

- [17] D. C. Wilcox, Turbulence modeling for CFD, 1998.
- [18] cfd-online.com, "CFD-Online," 2012. [Online]. Available: http://www.cfd-online.com/Wiki/Turbulence_free-stream_boundary_conditions. [Accessed 16 03 2012].
- [19] J. Andersson, "Simulation of wave induced forces on semi submerged horizontal cylinders using OpenFOAM," Department of Shipping and Marine Technology, Chalmers University of Technology, Gothenburg, 2011.
- [20] C. J. Mordhorst, "Investigation of open-source CFD software on shipyards," Department of Shipping and Marine Technology, Chalmers University of Technology, Gothenburg, 2011.
- [21] J. A. Alsgaard, "Numerical investigations of positon mode resonance in a moonpool using OpenFoam," NTNU Department of Marine Technology, Trondheim, 2010.
- [22] cfd-online.com, "CFD-Online," 2012. [Online]. Available: <http://www.cfd-online.com/Forums/OpenFOAM-solving/86855-near-wall-treatment-k-omega-sst.html>. [Accessed 15 05 2012].
- [23] F. OpenFOAM, "OpenFOAM USER MANUAL," 2012. [Online]. Available: <http://www.openfoam.org/docs/user>. [Accessed 26 04 2012].
- [24] T. Behrens, "OpenFOAM's basic solvers for linear systems of equations," 2009.
- [25] F. Juretic, "Error analysis in finite volume CFD," London, 2004.
- [26] E. van Vliet, "Dutch OpenFOAM® Users Group," 2010. [Online]. Available: <http://dutchopenfoamusers.nl/downloads/Eelco1.pdf>. [Accessed 15 04 2012].
- [27] O. M. Faltinsen, "Sea loads on ships and offshore structures," Cambridge, Press Syndicate of the University of Cambridge, 1990, pp. 87-88.

APPENDIX

APPENDIX I – MIN/MAX DRAG AND PRESSURE FOR CASES S0-S3

